We are IntechOpen, the world's leading publisher of Open Access books
Built by scientists, for scientists

4,800
Open access books available

122,000
International authors and editors

135M
Downloads

Our authors are among the

154
Countries delivered to

TOP 1%
most cited scientists

12.2%
Contributors from top 500 universities

CLARIVATE ANALYTICS
BOOK CITATION INDEX
INDEXED

WEB OF SCIENCE™

Selection of our books indexed in the Book Citation Index in Web of Science™ Core Collection (BKCI)

Interested in publishing with us?
Contact book.department@intechopen.com

Numbers displayed above are based on latest data collected.
For more information visit www.intechopen.com

Chapter 1

Strain Effect in Epitaxial Oxide Heterostructures

Abhijit Biswas and Yoon Hee Jeong

Additional information is available at the end of the chapter

http://dx.doi.org/10.5772/intechopen.70125

Abstract

In recent decades, extensive studies have been conducted on controlling and engineering novel functionalities in transition metal oxide (TMO) heterostructures by epitaxial strain. In this chapter, we discuss popular transition metal oxide thin films in the context of various research fields that are extensively studied in condensed matter physics. These materials include $La_{1.85}Sr_{0.15}CuO_4$ (a high temperature superconductor), $SrRuO_3$ (a highly conductive ferromagnetic metal), $La_{0.67}Sr_{0.33}MnO_3$ (a colossal magnetoresistive ferromagnetic metal), $BiFeO_3$ (a multiferroic oxide), $LaAlO_3$-$SrTiO_3$ (a conductive oxide interface), and $LaNiO_3$ (a strongly correlated metal). We focus on the appearance of novel functional properties from imposing epitaxial strain (compressive or tensile strain caused by the use of various lattice-mismatched substrates) on these films that cannot be observed in their bulk form. Subsequently, the intrinsic mechanisms for these novel phenomena are discussed based on experimental observations and theoretical modelling. We conclude that by using epitaxial strain, not only can thin film functionalities be tuned but many novel correlated phenomena can also be created. We believe that our collective efforts on the strain engineering of various transition metal oxide thin films will provide an insightful description of this emerging subject from a fundamental physics and nanoscale device applications point of view.

Keywords: oxides, substrates, thin films, strain effect, transport properties

1. Introduction

Matter can primarily be classified into three states: (1) gaseous, (2) liquid, and (3) solid (or condensed). In gaseous phases, the interactions among particles (atoms, molecules and ions) are very weak, and therefore they move freely. In liquid phases, the interactions between particles are comparatively strong. In solids, particles are closely packed or condensed, making the interactions between them the strongest compared to the other two states of matter.

INTECH
open science | open minds

© 2018 The Author(s). Licensee InTech. This chapter is distributed under the terms of the Creative Commons Attribution License (http://creativecommons.org/licenses/by/3.0), which permits unrestricted use, distribution, and reproduction in any medium, provided the original work is properly cited. CC BY

Condensed matters (solids) are mostly crystalline; i.e., they have a periodic arrangement of atoms, ions or molecules. Depending on the periodicity of the atoms, they form different crystal structures. In nature, there are seven types of lattice structures: cubic (e.g., $SrTiO_3$), triclinic (e.g., $FeSiO_3$), monoclinic (e.g., $BiMnO_3$), orthorhombic (e.g., $GdFeO_3$), tetragonal (e.g., $BaTiO_3$), rhombohedral (e.g., $BiFeO_3$), and hexagonal (e.g., $YMnO_3$). Moreover, completely disordered systems displaying non-periodicity of atoms are called non-crystalline amorphous solids (e.g., glass). In reality, both types of systems show complex physics and chemistry with an immense number of functionalities [1].

Irrespective of their structural symmetry, three types of crystalline solids can be found either naturally or artificially, i.e., made in the laboratory. These include polycrystals, single crystals, and thin films. Polycrystalline materials are composed of many crystallites of various sizes that are oriented randomly (**Figure 1a**). Due to the random orientation of crystallites, they have many crystallite grains (~1 μm in size) with grain boundaries, twin boundaries and high porosity. As a result, polycrystals are occasionally considered dirty materials, and they show unusual behaviors at low temperature due to disorder. Polycrystals can be nearly several centimeters in size. Typically, the "solid-state reaction" method is used to synthesize polycrystalline materials [2].

Single crystals, in contrast, contain uniform orientations of their crystal lattices up to their edges, even at the macroscopic level; hence, there are no grain boundaries (**Figure 1b**). Therefore, it becomes easy to determine the various directions of a crystal and measure its properties along a particular direction. As a result, single crystals are regarded to be the cleanest and are very popular among the material science community as they reflect the exact properties of a material. Single crystals are nearly a few mm in size. For the most part, the floating-zone method, Czochralski method and Bridgman-Stockbarger method are used to grow high-quality single crystals [3]. A detailed analysis of these methods is beyond the scope of this chapter.

Thin films consist of very few layers of a solid material. They are typically deposited on structurally compatible metal oxide substrate surfaces (**Figure 1c**) by various thin-film deposition techniques [5]. Details about various thin-film deposition techniques are discussed later in

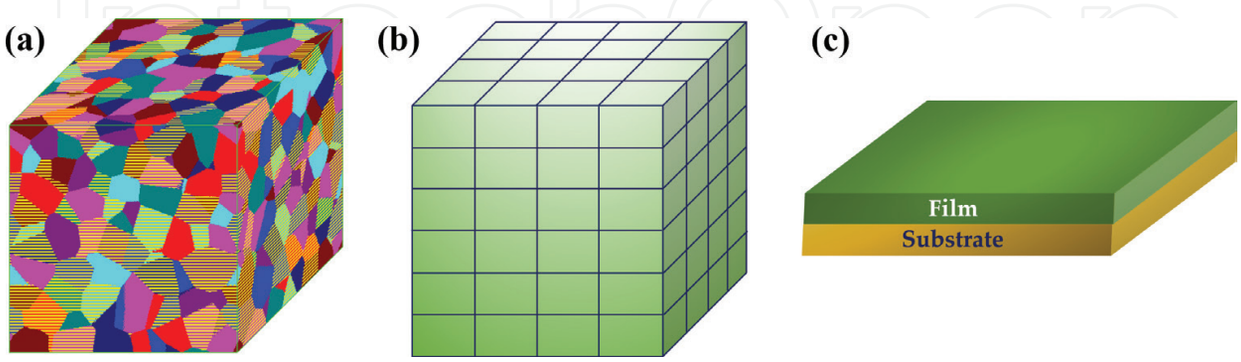

Figure 1. Schematics of a (a) polycrystal, (b) single crystal, and (c) thin film. Polycrystals have many grains, whereas the crystal orientation in single crystals is uniform. Moreover, thin films are grown on structurally compatible metal oxide substrates. Polycrystalline figure was taken from Ref. [4].

this chapter. Thin films are those with thicknesses ranging from a few angstroms to several nanometers (~4 Å to 1000 nm). Most thin films are made of oxides, particularly transition metal oxides (TMOs).

TMO thin films are one of the most investigated research topics in condensed matter physics as they show a variety of phenomena, e.g., metal insulator transitions (MIT), high-temperature superconductivity (HTSC), colossal magnetoresistance (CMR), and multiferrocity (coexistence of magnetism and ferroelectricity), as well as those exhibited by high-mobility two-dimensional electron gases (2DEGs), topological insulators (TI), and quantum spin-liquids (QSL) [6–20]. In TMOs, the *d*-orbital electrons of transition metal elements play a crucial role in determining the physical properties of a compound through the interplay between spin, lattice, charge, and orbital degrees of freedom (**Figure 2a**) [21–24]. Among the various types of TMOs, perovskites are a class of materials that shows almost all the properties mentioned above. They have been a deeply researched topic among physicists owing to their simple crystal structure (**Figure 2b**) [25, 26].

Perovskites, named after the Russian Mineralogist Count Lev Aleksevich von Perovski, have a general unit cell crystal structure of the ABO_3 type, where the A-site is an alkaline earth or rare earth metal and the B-site is a transition metal element (e.g., Fe, Co, Ni, Mn, Ti, Ru, and Ir). The structure can easily accommodate a wide range of valence states in both A- and B-sites (e.g. $A^{+1}B^{+5}O_3$, $A^{+2}B^{+4}O_3$, and $A^{+3}B^{+3}O_3$); so the variety of perovskite oxides is unlimited; for example, manganites, ruthenates, nickelates, titanates, and iridates [25]. $CaTiO_3$ was the first perovskite discovered by Gustav Rose in 1839 from samples found in the Ural Mountains in Russia. The B-site cation of ABO_3 perovskites is surrounded by six O anions, forming a corner-shared BO_6 octahedron (**Figure 2c**). This octahedral cage is the most important part of the crystal structure of these materials because the hopping of electrons from one *d*-orbital of the transition metal element to another *d*-orbital depends on the shape, size and position of this octahedron; thus, it affects the physics and chemistry of the material and the appearance of variety of phenomena [21–24].

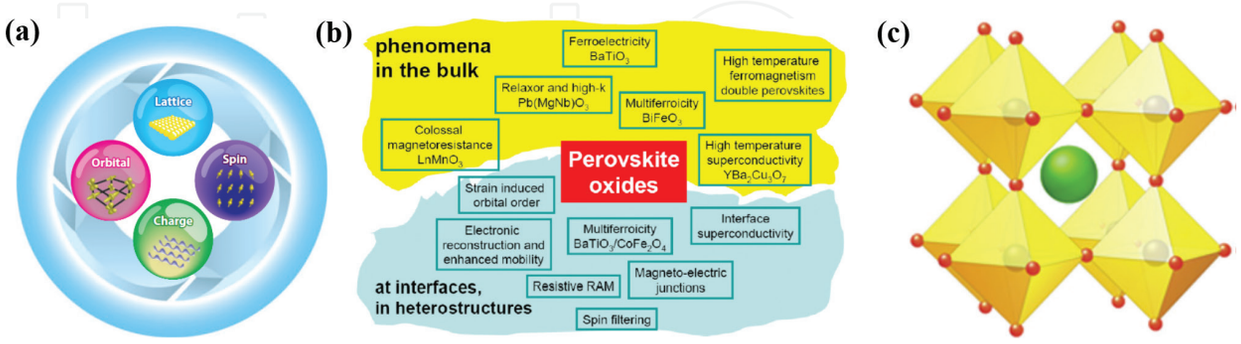

Figure 2. (a)-(b) Electronic and structural degrees of freedom in transition metal oxides and their interplay show a variety of correlated multifunctional phenomena in perovskite oxides, for both bulk and heterostructure thin films. (c) Schematic representation of a typical ABO_3 perovskite structure (e.g., $SrTiO_3$). Sr-cation is at the center; Ti-cation is surrounded by six O-anion forming TiO_6 octahedra cage. Reprinted with permission from [11, 20, 26]. Copyright 2012 Elsevier Ltd; Copyright 2014 Annual Reviews; Copyright 2008 IOP Publishing Group.

In bulk polycrystals and single crystals, the shape, size and position of the BO_6 octahedra can be manipulated externally by inducing chemical pressure (replacing A-site or B-site cations with other transition metal elements), or by partial oxygen pressure (changing the pressure from the atmospheric one) [6]. Ceramic materials fail structurally under modest strain (typically < 0.1% under strain) as these materials are brittle and thus will crack under this magnitude of strain, limiting the ability of routes involving chemical substitutions to control these materials. Cations with different sizes lead to the distortion of the crystal lattice, which is usually quantified as the Goldsmith tolerance factor [27] t_f, given by

$$t_f = \frac{r_A + r_O}{\sqrt{2}(r_B + r_O)} \quad (1)$$

where r_A, r_B, and r_O represent the ionic radii of ions A, B and O, respectively. The stability and distortion of a crystal structure is indicated by the value of t_f. For a perfect cubic structure, t_f is 1. Structure still remains cubic for $0.89 \leq t_f \leq 1.0$ [26]. For more lower value of t_f it forms other types of crystal structures, resulting in structural transitions to orthorhombic, or rhombohedral states that have lower symmetry than the cubic state.

However, as a result of chemical substitutions, disorder is introduced into the materials, which in most cases suppresses and even destroys the properties of a material. These difficulties can be overcome in a unique way in thin films by a disorder-free clean route approach. This can be achieved by growing thin films on substrates that are structurally compatible but have different cubic (pseudo-cubic) lattice constants. This is termed "strain engineering" in epitaxial thin films [28]. Once a strain effect is induced in a film, due to the change of energy scales of various degrees of freedoms (lattice, charge, spin, and orbital), it shows novel properties that cannot be found in parent bulk compound. This means that novel quantum-correlated phenomena can be obtained by the strain engineering of oxide heterostructures, which broadens the field and our understanding of condensed matter physics. In the next section, we will discuss how to grow such atomically controlled high-quality thin films and induce the strain effect in TMO heterostructure.

2. Thin film growth methods and substrates

In recent decades, significant advances have been made in synthesizing epitaxial thin films in the laboratory using various deposition techniques [5]. These methods are: (1) pulsed laser deposition (PLD), (2) molecular beam epitaxy (MBE), (3) off-axis radio frequency magnetron sputtering (RFMS), (4) metal-organic chemical vapor deposition (MOCVD), and (5) chemical solution deposition (CSD). By using these techniques, atomically controlled epitaxial thin films (*epi* means "above" and *taxy* means "in an ordered manner" in Greek), heterostructures and artificial superlattices can be grown. Among these techniques, PLD and MBE are the most popular ones adopted by the thin film community.

2.1. Pulsed laser deposition (PLD)

In 1986, the successful growth of HTSC $YBa_2Cu_3O_{7-\delta}$ (YBCO, T_{SC} ~90 K) thin films by the PLD technique by Dijkkamp et al., generated great interest among the material science community,

as it provided an alternative method for making thin-film materials in the laboratory [29]. The PLD technique is probably the most commonly used method for growing oxide thin films [5, 30–32]. Films are grown inside a high-vacuum chamber. A homemade or commercially available polycrystalline target is ablated by an energy source (typically a KrF laser with a wavelength of 248 nm or a frequency-doubled Nd:YAG laser with a wavelength of 532 nm). When the target is ablated, it produces a highly energetic plasma plume from the target. This highly energetic plume contains ions and molecules that are then deposited onto the substrate surface, which is attached on a substrate holder and placed opposite the target along the same out-of-plane axis. The substrate temperature, which is controlled by a heater, is determined from outside the chamber using a pyrometer. The target-to-substrate distance is kept at ~40–50 mm as the dynamics and kinetics of the plume species are limited to a maximum critical distance from the target because of collisions. A schematic diagram of a PLD chamber is shown (**Figure 3a**) [33]. Gaseous atoms condense on a template created by the substrate to form a single crystal. During this process, one needs to fulfill the growing conditions, e.g., optimize the base pressure, gas (O_2, O_3, or Ar) pressure, substrate temperature, laser density, spot size, and substrate surface flatness. Since the whole process is a thermally non-equilibrium one, by tuning all these parameters and ultimately optimizing them, one can grow the highest quality atomically controlled epitaxial oxide thin films (**Figure 3b**) [15]. The *in-situ* growth process can be monitored in real time by using the reflection high-energy electron diffraction (RHEED) method.

The advantages of the PLD technique are: (1) *in-situ* stoichiometric transfer of composition from target to substrate; (2) compatible materials can be grown under oxygen pressures ranging from ultra-high vacuum (UHV) to atmospheric pressure; (3) materials ranging from ultra-thin homoepitaxial thin films to artificial superlattices can be grown with nanometer precision; (4) depending on the availability of the target material, a wide variety of films can be grown; and (5) materials are grown in a compact and inexpensive chamber. Furthermore, the disadvantages are: (1) sub-optimized growth conditions can lead to the non-stoichiometric films; and (2) due to the highly energetic plumes, macroparticles called "droplets" can be deposited on a substrate surfaces within a micrometer range [30]. Therefore, to grow the highest quality epitaxial thin films, one should be aware of these facts. There are many groups around the world who have been pioneers in growing artificial epitaxial single-crystalline thin films of the highest quality.

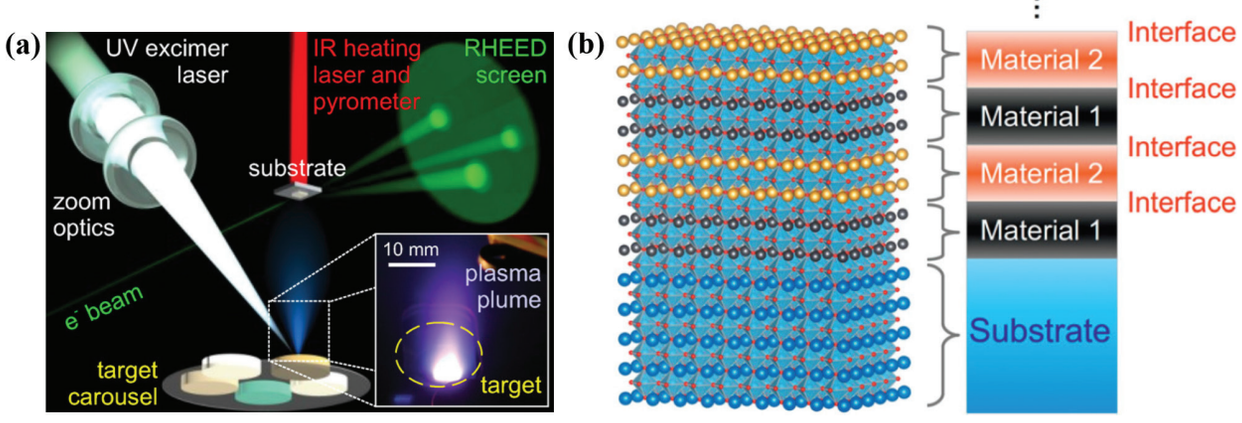

Figure 3. (a) Schematic diagram of a PLD chamber used for growing epitaxial oxide thin films. (b) Schematic of a layer-by-layer view of two different materials grown on a substrate. Reprinted with permission from Refs. [15, 33]. Copyright 2013 Materials Research Society; Copyright 2012 IOP Publishing Ltd.

2.2. Molecular beam epitaxy (MBE)

Molecular beam epitaxy (MBE) is also a method used to grow high-quality epitaxial thin films [5, 34]. It was invented in 1960s at Bell Labs by Arthur and Alfred Y. Cho [35]. The overall schematic of MBE is very similar to that of PLD thin film deposition. The only difference is the target material. Instead of a ceramic target, one uses "guns" called effusion cells (**Figure 4a**) [28, 36]. At the same time, one generates molecules from each cell using a highly intense laser beam (termed "atomic spray painting" by D. G. Schlom, a famous MBE thin film scientist) (**Figure 4b**) [28]. The spray duration is individually controlled for each beam by shutters. Once all the deposition conditions are satisfied, the ejected molecules travel to the substrate surface, condenses and form a single-crystalline thin film compatible with the substrate crystal structure. One of the main advantages of MBE thin film growth is its extreme cleanliness; i.e., no dirt particles (highly energetic species) or unwanted gas molecules can interfere with or contaminate the single-crystal thin film growth.

2.3. Substrate selection for epitaxial thin films

Substrates seem to be the basis of all thin film growth. Choosing a suitable metal oxide substrate is an important factor for growing high-quality epitaxial thin films as the structure and properties of a thin film depends on the underlying substrate and the interfacial interaction

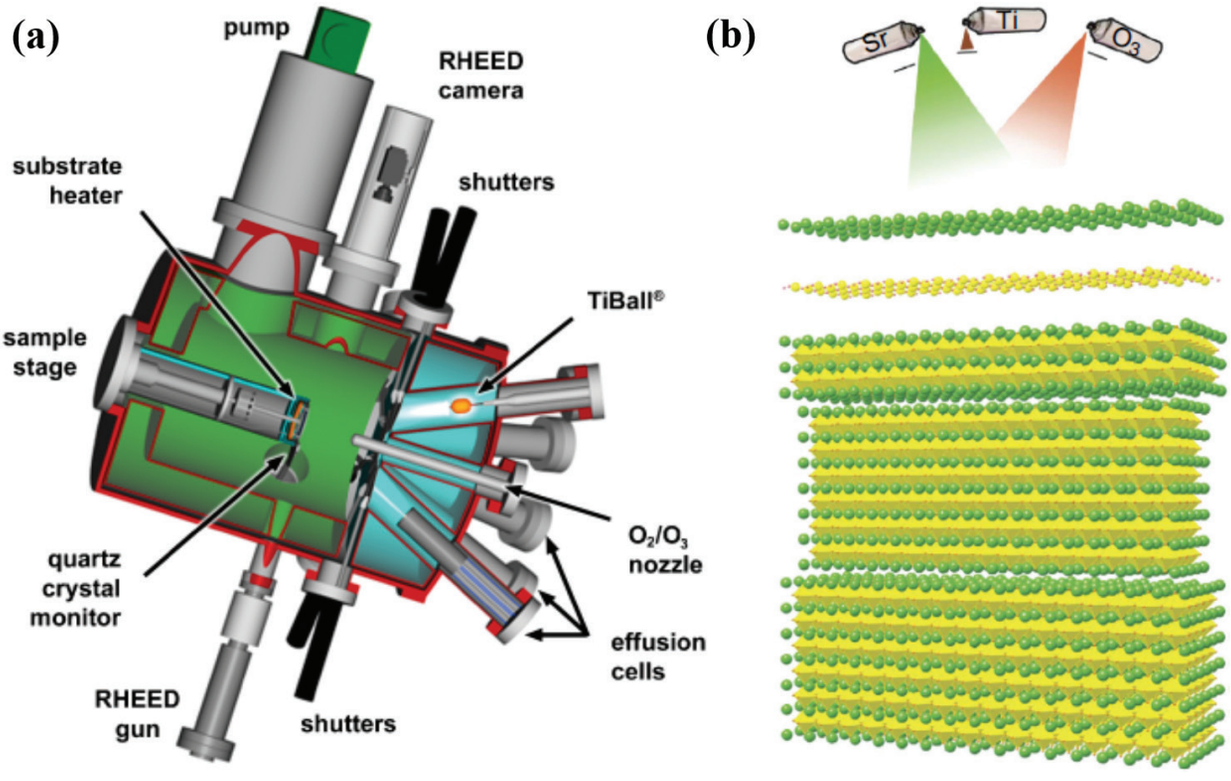

Figure 4. (a) Schematic diagram of a laser-MBE chamber for growing epitaxial thin films. (b) Schematic illustration of layer-by-layer MBE thin film growth, i.e., "atomic spray painting." Reprinted with permission from [28, 37]. Copyright 2008 The American Ceramic Society; Copyright 2014 Macmillan Publishers Limited.

between the substrate and film [38]. When choosing a metal oxide substrate for growing epitaxial films, one should consider the following factors:

1. Lattice matching between the substrate and film, which is important for the growth of most natural state films (structural compatibility).
2. No chemical reaction between the elements of the substrate and film (chemically compatibility).
3. Thermal-expansion matching between the substrate and film, as films are generally grown at high temperatures (good thermal-expansion match).
4. Surface quality of the substrate (e.g., free of cracks, unwanted particles, defects, and impure phases).

In most cases, the lattice constant and structure of a thin film should be compatible with those of the substrate to grow epitaxial films in their most natural state (**Figure 5a**). For most ABO_3 perovskites, their lattice constants range from 3.80 to 4.00 Å [39]. Fortunately, there are many perovskite single-crystal metal oxide substrates available commercially with lattice constants

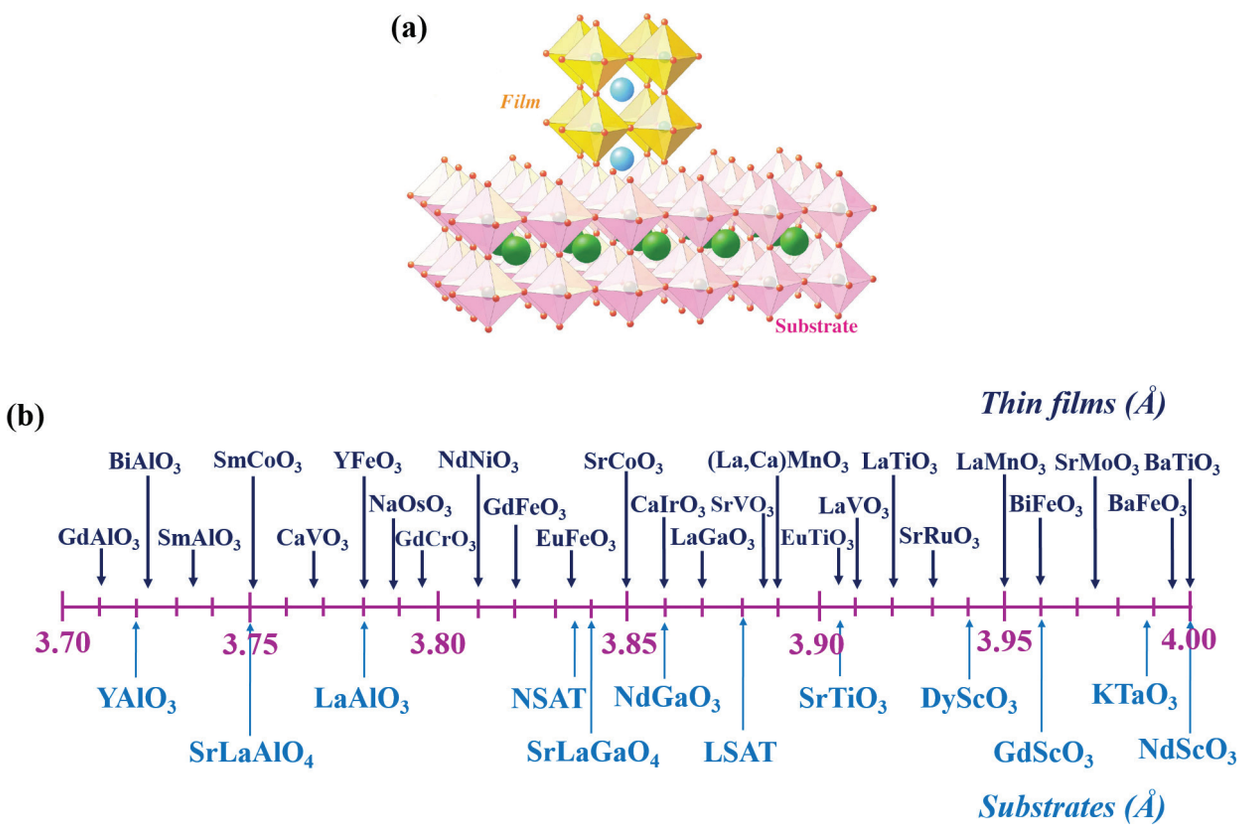

Figure 5. (a) Structural relationship between the substrate and film. For the most natural growth state of a film, a film's lattice constant (a_f) should be similar to the substrate's lattice constant (a_s), and the two should have structural compatibility. (b) List of cubic (pseudo-cubic) substrates and thin films within the lattice constant range from 3.70 to 4.00 Å. With a judicial choice of substrate, various atomically controlled high-quality thin films can be grown. Reprinted and adapted with permission from Ref. [41]. Copyright 2014 Materials Research Society.

ranging from 3.70 to 4.20 Å [28, 33, 40–42]. Among various available perovskite substrates, insulating $SrTiO_3$ is the most popular one. It has a cubic structure with a lattice constant of ~3.905 Å. There are also a broad range of substrates available with similar structures to that of $SrTiO_3$ while possessing different lattice constants and crystal orientations. These commercially available substrates include *RE*ScO_3 (*RE* = rare earths), $La_{0.18}Sr_{0.82}Al_{0.59}Ta_{0.41}O_3$ (LSAT), $NdGaO_3$, $SrLaAlO_4$, $LaAlO_3$, $SrLaAlO_4$, and $YAlO_3$ (**Figure 5b**). Thus, after careful consideration of all the important factors listed above and a film's lattice constant, it is easy to choose a substrate suitable for the epitaxial growth of thin films.

3. Strain in perovskite thin films

3.1. Strain engineering of perovskite thin films

Strain engineering is a unique way to create the novel functionalities in epitaxial oxide thin films [40–43]. From substrate-thin film relation point of view, when the lattice constant of a film (a_f) is dissimilar to the lattice constant a substrate (a_s), compression or elongation occurs within the film's crystal structure and thus elastic strain is induced in the film [41]. For cases of dissimilar lattice constants ($a_f \neq a_s$), the structure of the thin film tries to take the structure of the substrate, causing structural changes (mainly the change in BO_6 octahedron rotation, tilting, and distortion, and/or the change in B—O bond length) to occur from the original atomic position. This is defined as the typical strain effect in thin films. Quantitatively, the amount of strain (ε) induced in a film is defined as

$$\epsilon = \left(\frac{a_s - a_f}{a_f}\right) \tag{2}$$

where a_s is the substrate lattice constant and a_f is the film lattice constant.

Generally, compressive strain (**Figure 6a**) is induced in a film when $a_f > a_s$, whereas tensile strain (**Figure 6b**) is induced in a film when $a_f < a_s$. Under these epitaxial strain scenarios, the properties of functional oxide thin films can be drastically altered. Currently, the strain (ε) of ~2–3% is quite common in epitaxial oxide thin films, with highest strain to date of ~6.5% being imposed on multiferroic $BiFeO_3$ films grown on a highly lattice-mismatched (1 1 0) $YAlO_3$ substrate [43]. Thus, elastic strain is a viable route to observe materials with exceptional properties that cannot be observed in their bulk form by any other means [44, 45]. Although it looks simple, the intrinsic mechanism of the appearance of novel functionalities induced by the strain effect is quite complex to understand. In the next section, we briefly discuss about the intrinsic mechanism of the strain effect in perovskite thin films.

3.2. Mechanism of the strain effect in perovskite thin films

In post-Moore era, electronic devices with multifunctionality may offer a new alternative to replace the current silicon-based technology because the additional value the devices would

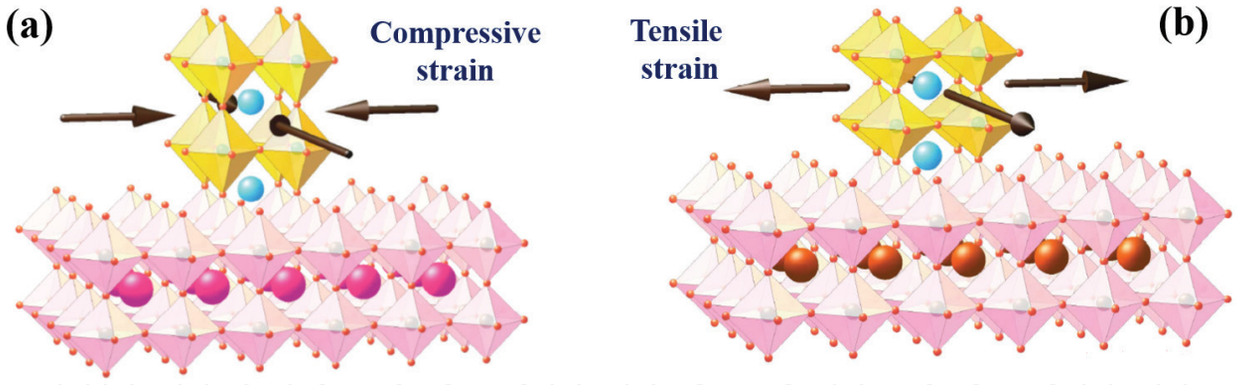

Figure 6. "*Strain engineering*" of perovskite heterostructures. (a) Compressive and (b) tensile strain is induced in a film through the use of various lattice-mismatched substrates. For compressive strain, $a_f > a_s$, whereas for tensile strain, $a_f < a_s$. In principle, for compressive strain, a thin film's lattice is compressed along the in-plane direction, and expanded along the out-of-plane direction. On the other hand, for tensile strained films, lattices expand along the in-plane direction and shrink along the out-of-pane direction. Reprinted with permission from Ref. [41]. Copyright 2014 Materials Research Society.

generate from multifunctionality may create an economically viable path superseding the miniaturization limit of silicon electronic devices. In this perspective, oxide electronics based on multifunctional properties of transition metal oxides looks promising [46, 47]. Even more exciting is the fact that advanced thin film growth techniques with atomic controllability provide further opportunities to design and synthesize artificial complex transition metal oxide heterostructures and superlattices to bring forth emergent physical properties, normally not seen in bulk states. However, despite the rapid progress and tremendous success in obtaining novel functionalities by the strain engineering of epitaxial oxide heterostructures, there is no general rule or theory available till date for predicting a material's electronic, magnetic, or other functional properties. This is perhaps due to a lack of knowledge about fully resolved atomic structures, especially the position of non-trivial oxygen atoms, as no experimental tool has yet been developed for the direct observation of oxygen atoms. In view of the lack of an experimental tool of this kind for transition metal oxides, electronic structure calculations could play a role instead. J. M. Rondinelli and N. A. Spaldin's recent article is particularly insightful in this regard, and we follow them briefly in this section [48].

The detailed structural distortion obtained by the movement of oxygen atoms due to strain is highly significant and it has a strong influence on the electronic properties of TMOs. In fact, just a small modification in an atomic structure would change the relevant energy scales (lattice, charge, spin, and orbital) and it is hard to predict functionalities as material properties are strongly dependent on the competition between these energy scales. To illustrate the effects of structural distortions in thin films, let us start with the ideal ABO_3 perovskite structure which is a simple cubic one with space group $Pm\bar{3}m$. The most important part of this structure is its corner-shared BO_6 (*B* = transition metal) octahedron, which results in an O—B—O—B chain with a 180° B—O—B bond angle (**Figure 7a**). There are very few systems that adopt this cubic structure (e.g., $SrTiO_3$); however, in practice, most perovskites show structural distortions that lower their symmetry from that of a highly symmetric cubic structure.

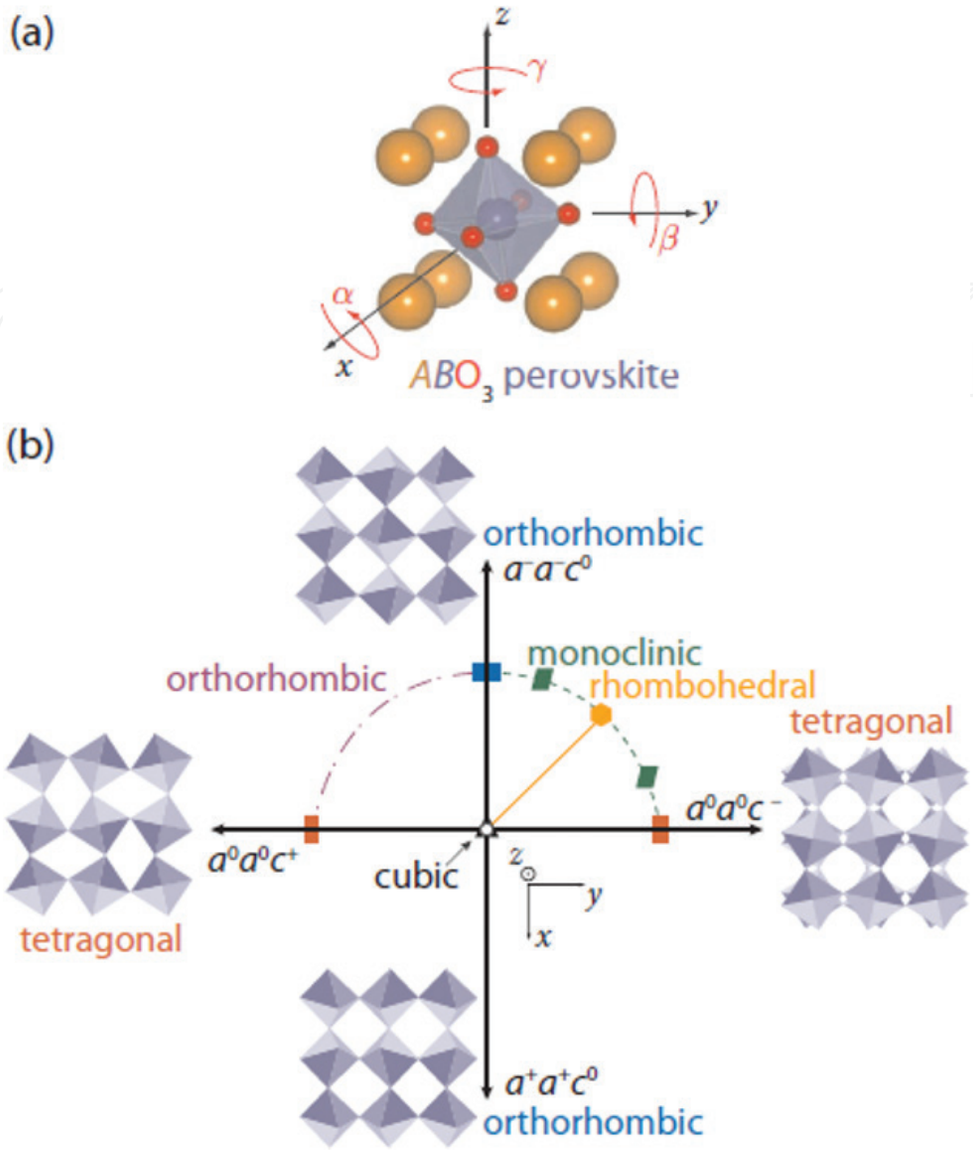

Figure 7. (a) The ideal ABO_3 perovskite crystal structure showing tilt in all three directions. (b) Distortion of BO_6 octahedra along various directions, lowering the symmetry of the cubic structure and forming other crystal structure. The +ve sign indicates in-phase rotation (c^+), and the −ve sign indicates out-of-phase rotation (c^-). Reprinted with permission from Ref. [48]. Copyright 2011 WILEY-VCH Verlag GmbH & Co. KGaA, Weinheim.

Rotations or tilts of BO_6 octahedra around the high-symmetry axes are the most common distortions in perovskite structures [49–51]. These are conveniently described by the Glazer notation [52, 53] and written as $a^{\#}b^{\#}c^{\#}$, where a, b, and c are the axes around which rotation occurs and the superscripts indicate whether the octahedral rotation is in phase (+) or out of phase (−). Thus, a, b, and c are not identical with the lattice constants; instead, they indicate that the nearest neighbor transition metal distances along that direction are equivalent. As perovskites are three-dimensional systems, a rotation or tilt in one direction restricts the rotation or tilt in other directions. Depending on the rotation or tilt of the BO_6 octahedra, the cubic structure can deform, leading to the symmetry lowering of other crystal structures (**Figure 7b**) [48–51].

This structural distortion is imposed on a thin film by the appropriate choice of lattice-mismatched substrates. It is widely believed that the strain imposed by film-substrate lattice mismatch generally changes the in-plane lattice parameter, but exactly what occurs still remains unclear and moreover is difficult to determine experimentally. Two possibilities remain: (1) changes in the in-plane lattice parameter are offset by changes in the in-plane metal-oxygen B—O bond lengths (**Figure 8a** and **b**), or (2) while keeping the B—O distance fixed, the lattice mismatch is offset by a change in magnitude of the tilt patterns through the rigid rotation of the BO_6 octahedron (**Figure 8c** and **d**). This is highly significant as, for example, the magnitude and symmetry of a crystal field are affected by changes in the B—O bond length, whereas the strength and sign of a superexchange interaction are affected by changes in the B—O—B bond angle [48].

Quantitatively, changes in the B—O bond length and B—O—B bond angles of octahedra affect the bandwidth (W) of ABO_3 perovskites as follows:

$$W \propto \frac{\cos\psi}{d^{3.5}} \tag{3}$$

where $\psi = (\pi - \phi)/2$ is the buckling deviation of the B—O—B bond angle ϕ from π and d is the B—O bond length (**Figure 8e**) [54]. Due to rigidity, it is hard to change the B—O bond-length. Thus, as a result of imposed strain, octahedral rotation and tilt angle changes, the electron hopping changes within the d-orbitals and thus changes a material's functionalities. Changes in the bandwidth also affect the effective correlation as in general changes in these energy scales cause the appearance of novel functionalities in oxide heterostructures under strain.

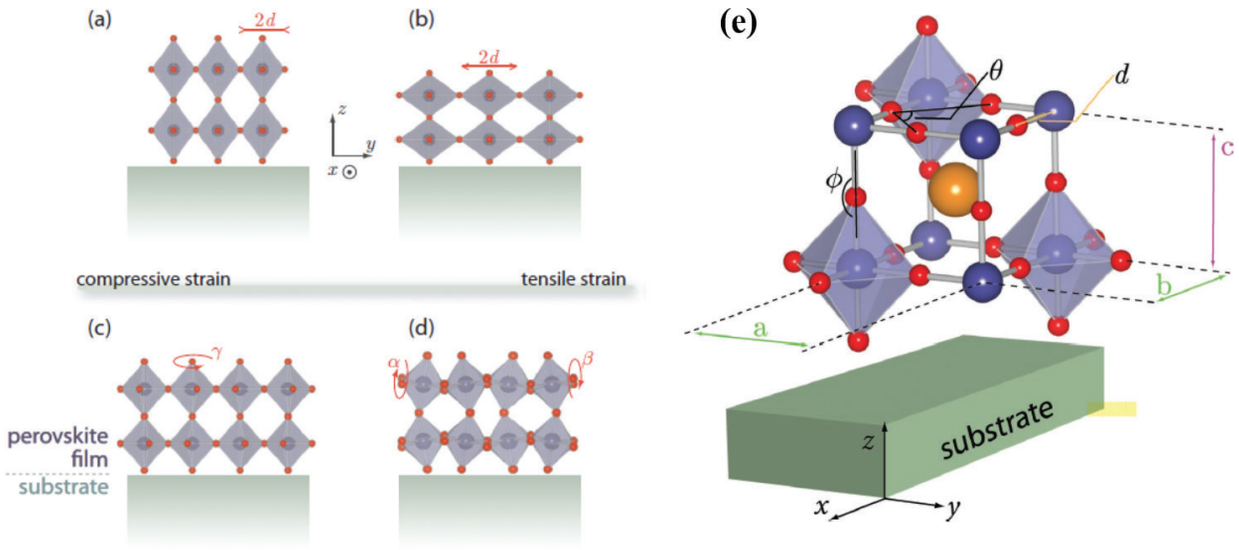

Figure 8. (a) Contraction and (b) elongation of B—O bond lengths, d, in a coherently strained perovskite film. Contraction is due to compressive strain, whereas elongation is due to tensile strain. Alternatively, change in the in-plane lattice parameters are due to the rotation of octahedra (c) perpendicular to the plane of the substrate or (d) about an axis parallel to the plane of the substrate. (e) Rotation (θ) and tilt (ϕ) angle used to describe the substrate-induced changes of octahedra. Reprinted with permission from Ref. [48]. Copyright 2011 WILEY-VCH Verlag GmbH & Co. KGaA, Weinheim.

Along with these changes in bond length, bond-angle and crystal symmetry that determine changes in the in-plane lattice parameters, another possibility for substrate-induced changes in lattice parameter remains: the defect stoichiometry or defect concentration of the material. Defect concentration, especially the oxygen concentration, is particularly important as films are generally grown under the high oxygen pressure or high vacuum. To accommodate the strain energy, it is easy to form oxygen vacancies. It is known that the higher the concentration of oxygen vacancies, the larger the lattice constants [55]. Since strain is induced by various lattice-mismatched substrates, it is difficult to establish whether changes in defect concentration are an intrinsic thermodynamic response due to strain or if they arise due to an extrinsic effect during the growth process.

4. Material properties tuned by epitaxial strain

4.1. A high temperature superconductor: $La_{1.85}Sr_{0.15}CuO_4$

In 1986, the discovery of HTSC in the cuprate oxide family by Bednorz and Müller generated considerable interest within the material science community, both in fundamental and applied research, due to the possibility obtaining oxides that are room-temperature superconductors [56]. $La_{1.85}Sr_{0.15}CuO_4$ (LSCO) is one example of these oxides. La_2CuO_4 is an antiferromagnetic insulator, but upon doping divalent Sr^{2+} ions in the trivalent La^{3+} site, magnetism is suppressed, and the compound makes a transition from an insulating to a superconducting state [57]. LSCO has a K_2NiF_4-type tetragonal structure with bulk lattice constants of a = 3.777 Å and c = 13.226 Å and space group *P42/ncm* (**Figure 9a**) [58]. It has quasi-two-dimensional copper-oxygen (Cu—O) planes, and superconductivity occurs within these planes [59]. In the bulk, around the optimal doping region, its maximum superconducting transition temperature is T_C ~25 K (**Figure 9b** and **c**) [60]. Its carrier doping remains within the Cu—O planes and the formation of electron pairs due to coupling between electrons and phonons seem to play a major role in achieving superconductivity [61]. Its critical temperature is controlled by either the density of electron pairs or the strength of electron pairing interactions [62].

In principle, external perturbation is applied to a material to enhance its functional properties, suggesting that substrate-induced strain might be a way to enhance the superconducting T_C of cuprates (**Figure 10a**) [63–70]. Indeed, Sato et al., and Locquet et al., grew $La_{2-x}Sr_xCuO_4$ (LSCO; x = 0.1, 0.15) thin films on two different substrates, such as (0 0 1) $SrTiO_3$ and (0 0 1) $SrLaAlO_4$ [63, 64]. Surprisingly, Locquet et al., observed that when films are grown on highly strained (0 0 1) $SrLaAlO_4$ substrates (a_s = 3.75 Å), which produces ~0.5% compressive strain onto these films, this amount of strain is enough to modify the superconducting T_C, making T_C almost double to its value found in the bulk, i.e., T_C ~49.1 K (**Figure 10b**) [64]. Independently, Sato, also reported the same study (**Figure 10c**) [69]. This is thought to be associated with strain-induced lattice deformation, which modifies the energy scales, leading to the formation and condensation of superconducting pairs. It was also observed that the residual resistivity value (ρ (0 K)) decreases as T_C increases [69]. More specifically, increasing T_C has a clear correlation with low residual resistivity. As stated by Sato, an increase in Cu—O bond length enhances the electrostatic potential at the Cu site relative to that at the oxygen site in the Cu—O plane.

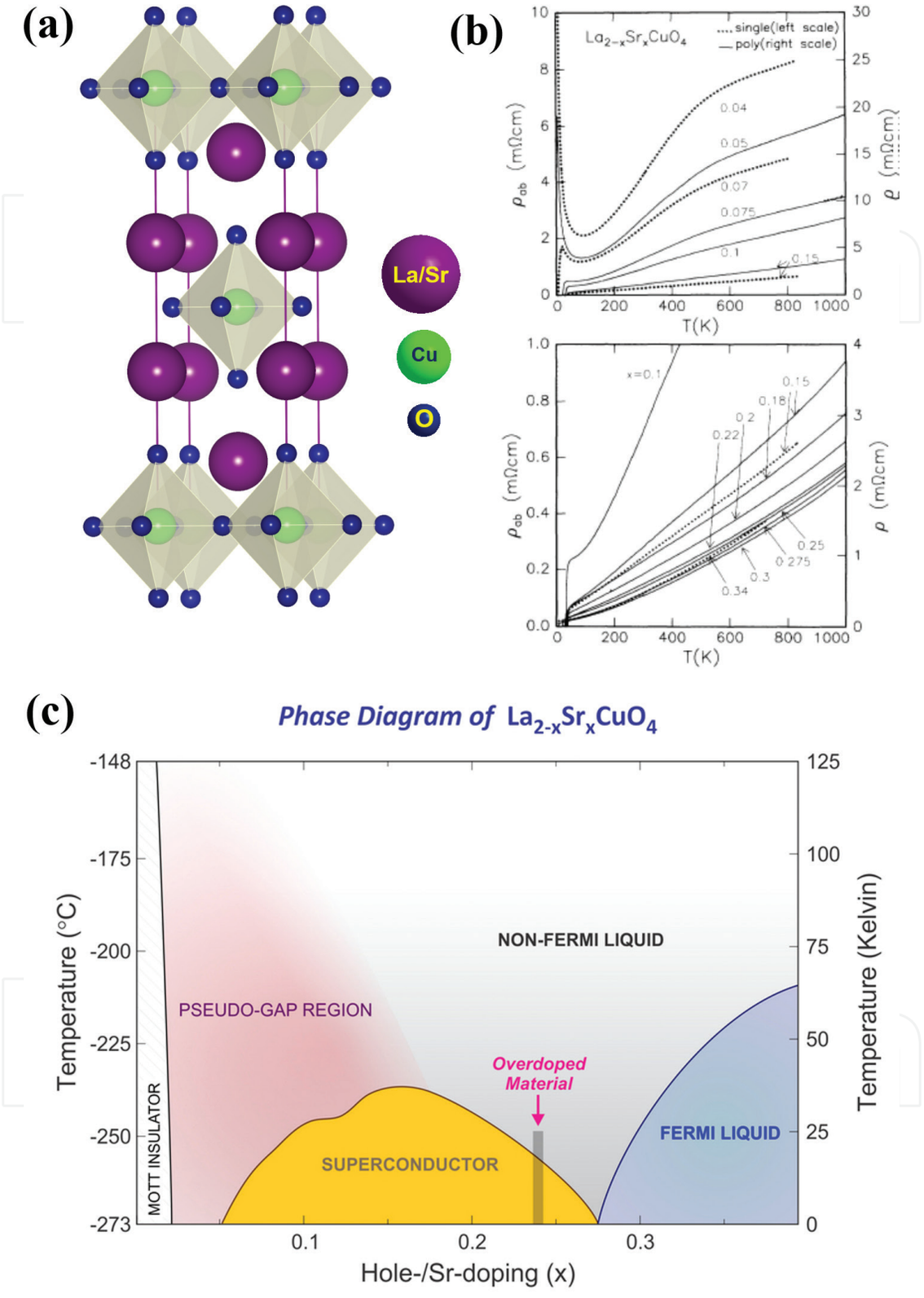

Figure 9. (a) Schematic representation of the K_2NiF_4-type tetragonal crystal structure of $La_{2-x}Sr_xCuO_4$ (LSCO) with lattice constants of $a = 3.777$ Å and $c = 13.226$ Å. (b) Resistivity of bulk single LSCO, showing the appearance of superconducting T_{SC} upon divalent Sr hole doping. (c) Sr hole doping dependence temperature vs. the material properties phase diagram of LSCO, showing that the system makes a transition from an antiferromagnetic insulator to a superconducting phase with the increase in Sr doping. Crystal structure was drawn using VESTA software. Reprinted with permission [57, 60]. Copyright 1992 American Physical Society; Copyright 2013 Macmillan Publishers Limited.

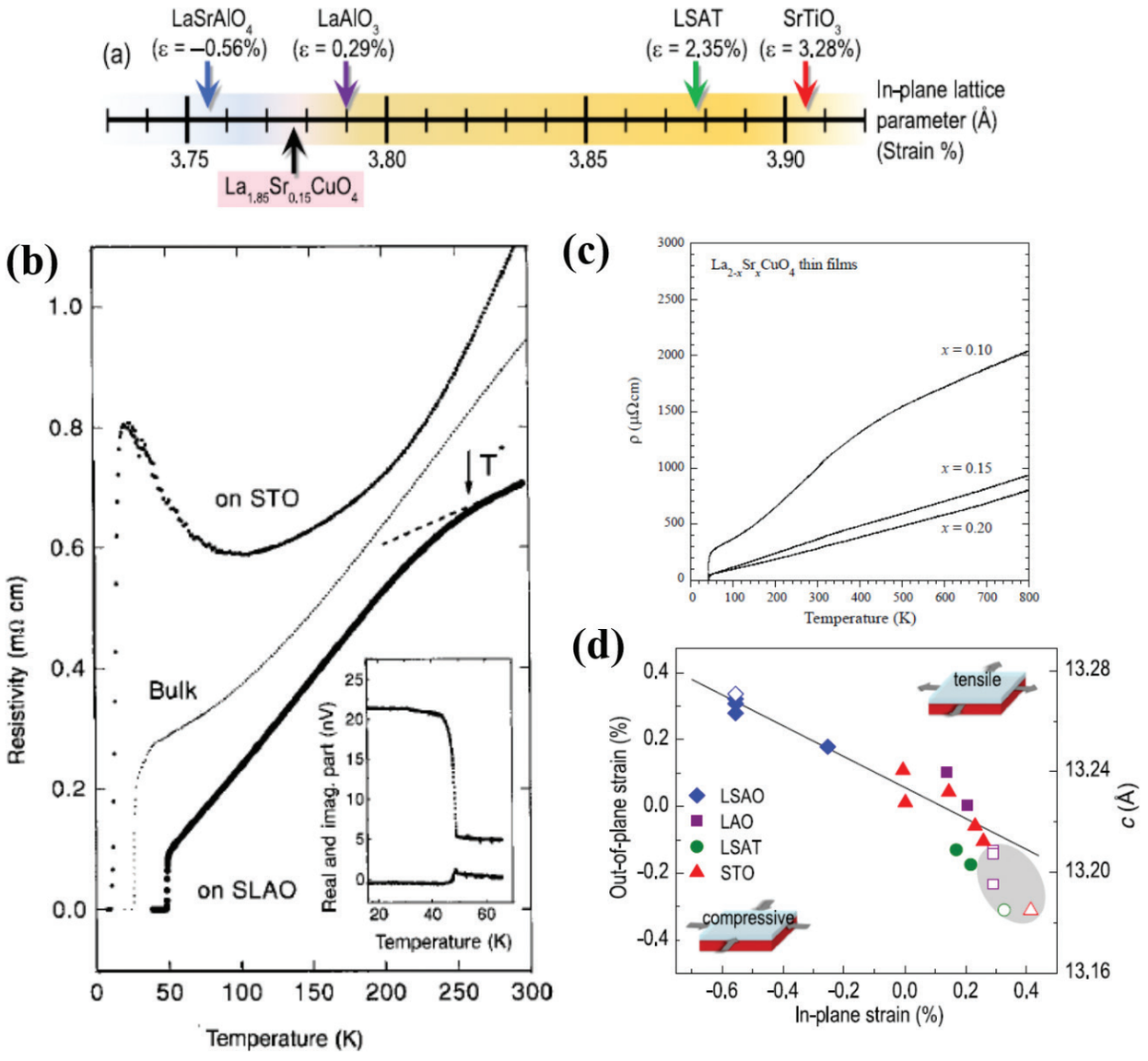

Figure 10. (a) In-plane strain and lattice parameters of the LSCO thin film and other perovskite substrates studied. (b) Strain-dependent resistivity (ρ) and superconductivity of LSCO films, showing that for tensile-strained films (on $SrTiO_3$ substrates), superconductivity occurs at T_C ~10 K, whereas for compressive-strained films (on $SrLaAlO_4$ substrates), the superconductivity transition temperature is doubled from the bulk value; i.e., T_C becomes ~49.1 K. (c) Superconductivity at T_C ~50 K for films grown on $LaSrAlO_4$ substrates with various amount of hole doping scenarios. (d) Changes in the *c*-axis lattice parameter and out-of-plane strain as a function of in-plane strain. The gray oval shape is the region where films do not show superconductivity. Reprinted with permission from Refs. [64, 69, 70]. Copyright 1998 Macmillan Publisher Ltd.; Copyright 2008 Elsevier Ltd.; Copyright 2015, AIP Publishing LLC.

Therefore, hole carriers are distributed more preferentially in itinerant states originating from the O 2p orbitals. As a result, antiferromagnetic spin fluctuation in the Cu—O plane is suppressed due to the reduction of the superexchange interaction between two adjacent Cu spins. Reduced spin fluctuation is the possible origin for reduction in ρ (0 K) and increase in T_C [69].

For compressively strained films grown on (0 0 1) $SrTiO_3$ substrate, which induced ~3% tensile strain on films, the T_C was found to be ~10 K [64]. Later, Božović et al., showed that with higher quality films (with much more oxygen intake as the films were annealed under an ozone atmosphere), T_C could reach up to ~40 K for tensile-strained films grown on (0 0 1)

$SrTiO_3$ substrates and ~51.5 K for compressive-strained films grown on (0 0 1) $LaSrAlO_4$ substrates [68]. Recently, Lee et al., also showed that oxygen vacancies and thickness-dependent strain relaxation indeed play a crucial role in increasing the superconducting T_C as lattice structures are highly sensitive to oxygen stoichiometry (**Figure 10d**) [70].

4.2. A highly conductive ferromagnetic metal: $SrRuO_3$

$SrRuO_3$ is one of the most promising oxide material among those used by thin-film researchers [71]. It is an itinerant ferromagnetic bad metal [72, 73]. Structurally, it has a $GdFeO_3$-type orthorhombic distorted perovskite structure at T = 300 K with lattice parameters of a = 5.5670 Å, b = 5.5304 Å, and c = 7.8446 Å and space group *Pbnm* (**Figure 11a**) [74]. This structure is converted into a pseudo-cubic (pc) lattice with a constant of $a_{pc} \sim 3.93$ Å $\left(a_c = b_c = \sqrt{a^2 + b^2/2} = d_{110}\right.$ and $\left.c_c = c/2 = d_{002}\right)$. Bulk $SrRuO_3$ shows structural phase transitions from orthorhombic to tetragonal at T = 547°C and then to cubic symmetry at T = 677°C, respectively [75]. This is associated with the occurrence of RuO_6 octahedral rotation, leading to a lowered structural symmetry from the ideal cubic perovskites.

In high-quality bulk single crystals, the ρ is ~200 μΩ cm with a mean free path of electrons of ~10 Å at T = 300 K (**Figure 11b**) [73]. $SrRuO_3$ shows a ferromagnetic transition at the Curie temperature T_C ~165 K (**Figure 11c**) with a magnetic moment of ~1.6 μ_B per Ru atom [76]. Although extensively studied, but the origin of its ferromagnetism, Stoner-type itinerant ferromagnetism vs. localized moment picture, is still under fierce debate because of contradicting experimental results and theoretical calculations [77, 78]. Due to its highly conductive nature and structural compatibility with other perovskite thin films, it is particularly interesting for its usefulness as a bottom electrode for $BiFeO_3$, $BaTiO_3$, or $Pb(Zr,Ti)O_3$ ferroelectric thin films used in electronic applications [79].

Eom et al. were the first to synthesize high quality metallic epitaxial $SrRuO_3$ thin films on various substrates [80]. The ferromagnetic transition temperature for these thin films were found be lower than the bulk value, T_C ~150 K, which is probably caused by the dimensionality and

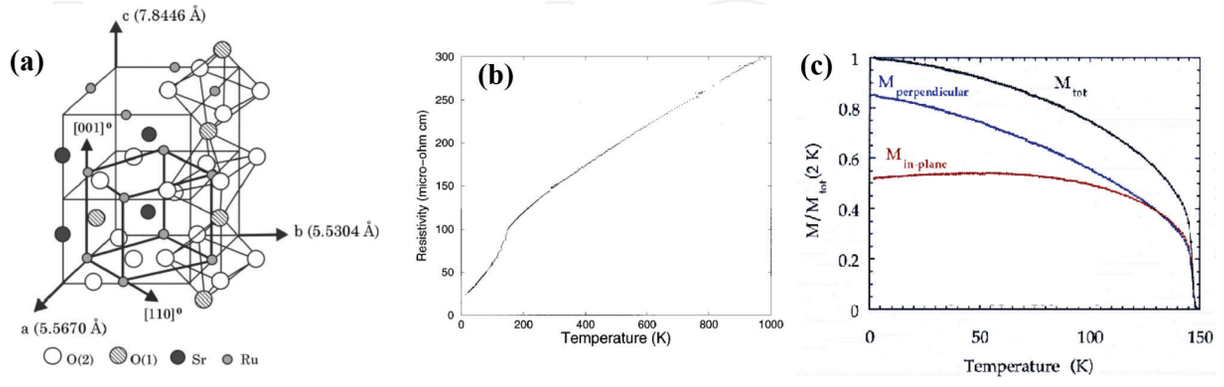

Figure 11. (a) Schematic view of the crystal structure $SrRuO_3$ showing both the orthorhombic and pseudo-cubic unit cell. Lattice parameters are a = 5.5670 Å, b = 5.5304 Å, and c = 7.8446 Å, with the pseudo-cubic (a_{pc}) one being ~3.93 Å. (b–c) Resistivity (ρ) and magnetization of $SrRuO_3$. The material was found be metal over the whole temperature range with ρ ~200 μΩ cm at T = 300 K. Magnetization measurement shows ferromagnetic ordering at T_C = 165 K. Reprinted with permission from Refs. [72–74]. Copyright 1996 IOP Publishing Ltd.; Copyright 1996, American Physical Society; Copyright 1999, American Institute of Physics.

strain effects [81]. Along with its electrode applications, due to its high metallicity upon ferromagnetic ordering, strain engineering of $SrRuO_3$ has become a popular research topic among thin-film scientists. Later, it has been found that the structural, metallic, and magnetic properties of $SrRuO_3$ thin films are highly sensitive to the substrate-induced strain (**Figure 12a**) [81–92].

The structural phase transition temperature (T_S) of $SrRuO_3$ is strongly affected by epitaxial strain. After imposing tensile strain on $SrRuO_3$ by growing films on (1 1 0) $DyScO_3$ substrates, an orthorhombic (stable in bulk phase) to tetragonal phase (stable at high temperature) transition could be observed at T = 300 K [84]. Strain imposed by substrates, induces additional rotation of RuO_6 octahedra, thus reducing the T_S [84, 86].

Transport wise, ρ at T = 300 K increases with the induced tensile strain (films grown on (1 1 0) $GdScO_3$ and (1 1 0) $DyScO_3$ substrates). The Ru—O—Ru bond angle is reduced when exerting tensile strain, which increases the effective correlation and thus reduces the bandwidth (W) (**Figure 12b**) [84]. Consequently, in the case of tensile-strained films, ρ has a higher value at T = 300 K compared to that of the most natural state of a film. On the other hand, it has also been found that for compressive-strained films (films grown on (0 0 1) $SrTiO_3$, (0 0 1) LSAT, and (0 0 1) $LaAlO_3$ substrates), ρ decreases, which is consistent with the increase in the Ru—O—Ru bond angle, decrease in effective correlation, and increase in bandwidth (W) (**Figure 12c**) [85]. The slight increase in the ρ of films grown on (0 0 1) $LaAlO_3$ substrates is associated with either the rough surface quality of the films caused by the twin structure of (0 0 1) $LaAlO_3$ or the films being fully relaxed on this substrate (**Figure 12d**) [85].

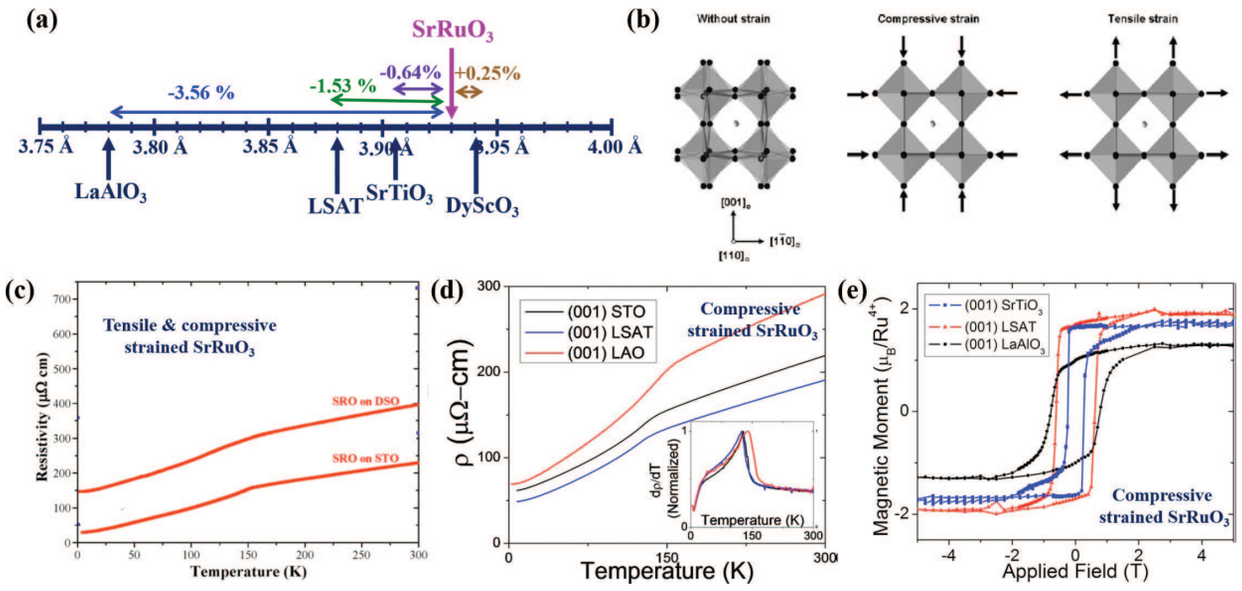

Figure 12. (a) Schematic illustration of the strain effect in epitaxial orthorhombic $SrRuO_3$ thin films. Films on $DyScO_3$ are subject to tensile strain, whereas films on $SrTiO_3$, LSAT, and $LaAlO_3$ undergo compressive strain. (b) Schematic representation of RuO_6 octahedral rotation from the bulk, due to both compressive and tensile strain. (c–d) Effect of tensile strain and compressive strain on the resistivity of $SrRuO_3$. For the tensile strain case, overall resistivity increases, while for the compressive-strained case, resistivity decreases from its bulk value. (e) Increase in saturation magnetization following the induction of compressive strain. The magnetic moment becomes ~2 μ_B per Ru atom, which is close to the theoretical value. Reprinted with permission from Refs. [84–86]. Copyright 2008 AIP Publishing LLC; Copyright 2010 AIP Publishing LLC; Copyright 2010 Wiley-VCH Gmbh & Co. KGaA.

Strain has definite effect on the magnetic properties of $SrRuO_3$. Inducing compressive strain on $SrRuO_3$ by using various lattice-mismatched substrates, e.g., (0 0 1) $SrTiO_3$, (0 0 1) LSAT, and (0 0 1) $LaAlO_3$, and its effect on magnetic properties has been investigated. The ferromagnetic T_C has a strong substrate dependence as it was found be T_C ~124 K for films grown on LSAT and T_C ~128 K for films grown on (0 0 1) $SrTiO_3$ [85]. It has been found that the saturated magnetic moment (M_S) increases from its bulk value and maximum of ~2 μ_B per Ru atom for films grown on (0 0 1) LSAT substrates (**Figure 12e**). For more compressive-strained films (those on (0 0 1) $LaAlO_3$), the M_S increases, possibly due to the deterioration in film quality caused by the twin structure of (0 0 1) $LaAlO_3$ substrates. The increase in M_S in compressive strained case is associated with the better alignment of moments in a low Ru^{4+} spin state. This higher value of magnetic moment was also expected based on the theoretical calculations [77].

Compressive and tensile strain-dependent physical properties have also been examined for the tetragonal phase of $SrRuO_3$. (1 1 0) $NaGaO_3$ substrates were used for imposing compressive strain, whereas (1 1 0) $GdScO_3$ substrates were used to induce tensile strain [90]. It has been found that tensile-strained films show low ferromagnetic ordering at T_C ~100 K, whereas compressively strained films show an almost bulk-like ferromagnetic transition at T_C ~155 K (**Figure 13**). Similar to the orthorhombic phase, compressive strain causes a lower residual resistivity ratio. The observations described above are associated with the deformation rather than the tilting of RuO_6 octahedra and thus the change in effective correlation [90–93].

4.3. A colossal magnetoresistive ferromagnetic metal: $La_{0.67}Sr_{0.33}MnO_3$

$La_{0.67}Sr_{0.33}MnO_3$ (LSMO) is an extremely important class of material in condensed matter physics [7, 94]. At T = 300 K, LSMO forms a rhombohedral crystal structure (a = 3.869 Å) with space group $R\bar{3}c$ (**Figure 14a**) [94]. Undoped $LaMnO_3$ is an antiferromagnetic insulator below T_N = 139.5 K [95]. Upon hole doping with divalent Sr^{2+} in place of La^{3+}, it becomes a ferromagnetic metal (**Figure 14b**) [96]. Doped LSMO is a mixed valence compound with Mn^{3+} ($3d^4$) and Mn^{4+} ($3d^3$). The change in its magnetism was well explained by the double-exchange hopping mechanism [96]. It is a highly conductive oxide that is useful as a bottom electrode for thin film device applications. It shows ferromagnetic ordering above room temperature with T_C ~360 K (**Figure 14c**) [97], having a magnetic moment of ~3.6 μ_B per Mn ion [98]. Its ρ changes greatly with the application of a magnetic field and shows colossal magnetoresistance (CMR; $\Delta\rho/\rho > 10^6$%) (**Figure 14d**) [97], which is important in commercial applications, including magnetic field sensors, "read" heads of magnetic hard-disk drives and non-volatile magnetic random access memory (MRAM). Its half metallic behavior—i.e., spins are fully polarized within one band structure whereas others are empty—is highly important for spintronic applications [98]. It also shows compositional- and temperature-dependent MITs (**Figure 14e**) [99].

Due to its rich electronic and magnetic phase diagram (**Figure 14e**) [99], it is highly desirable to investigate the change in functionalities or appearance of novel states in LSMO by inducing the strain effect. Several groups have reported on the effect of strain on the electronic and magnetic properties of LSMO [100–111]. To observe the strain-dependent magnetic phase diagram, Tsui et al., grew epitaxial LSMO thin films on various substrates, such as (0 0 1) $LaAlO_3$, (1 1 0) $NdGaO_3$, (0 0 1) LSAT, and (0 0 1) $SrTiO_3$ [103]. By using four different substrates, the

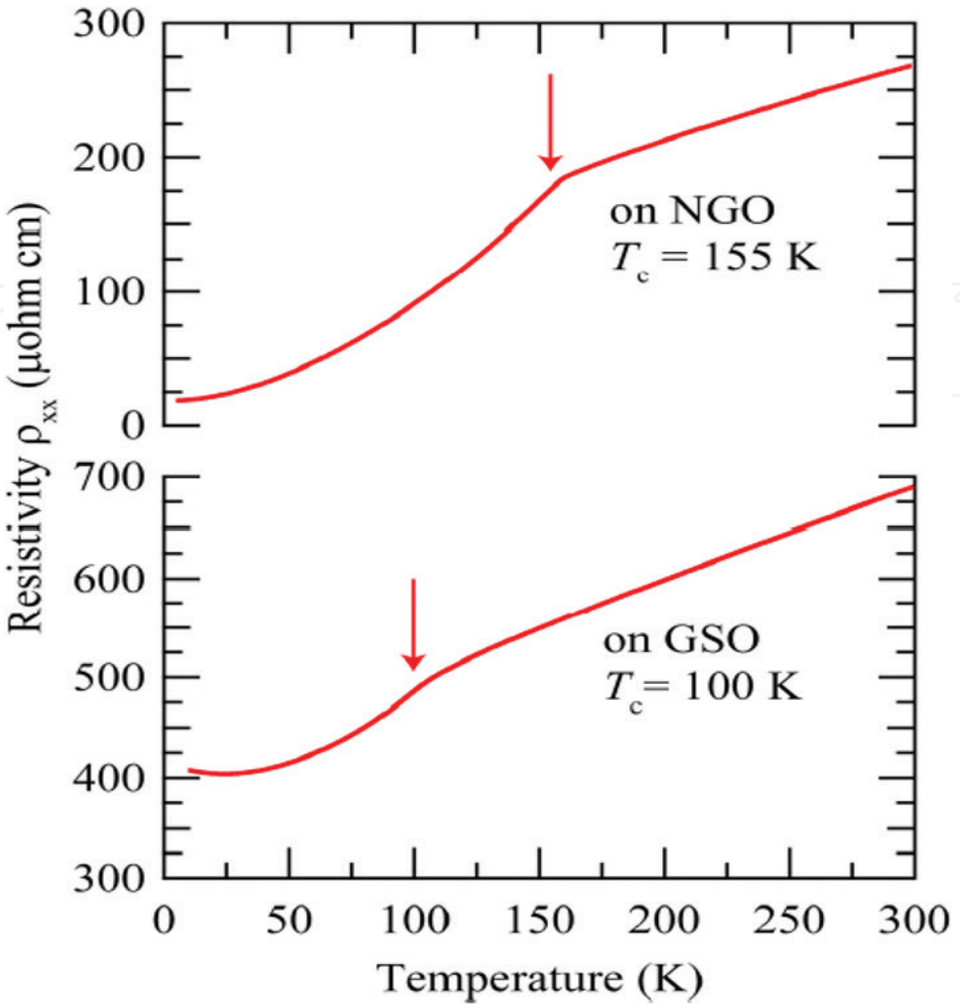

Figure 13. Compressive (on $NdGaO_3$) and tensile (on $GdScO_3$) strain-dependent resistivity of tetragonal phase $SrRuO_3$ thin films. A striking feature was obtained in magnetic ordering. For tensile-strained films (on $GdScO_3$), resistivity is higher than the bulk value and the magnetic ordering temperature is reduced with ferromagnetic T_C ~124 K. For compressive-strained film (on $NdGaO_3$), resistivity and magnetic ordering are very close to the bulk values with ferromagnetic T_C ~155 K. Reprinted with permission from Ref. [90]. Copyright 2013 AIP Publishing LLC.

strain ranged from compressive to tensile strain as follow; −2.0% compressive strain for films grown on (0 0 1) $LaAlO_3$, −0.25% compressive strain for films grown on (1 1 0) $NdGaO_3$, +0.25% tensile strain for films grown on (0 0 1) LSAT, and +0.85% tensile strain for films grown on (0 0 1) $SrTiO_3$. Compressively strained films on (0 0 1) $LaAlO_3$ substrates show in-plane compression and out-of-plane expansion in their lattice parameters. In contrast, tensile-strained films on (0 0 1) $SrTiO_3$ show the opposite effect. For films grown on the other two substrates with very low strain, they show very weak out-of-plane expansion in their lattice parameters. For compressively strained films on (0 0 1) $LaAlO_3$ substrates, there is a strong suppression of T_C from its bulk value; i.e., T_C is reduced from 360 to 300 K. There is an increase in in-plane magnetization compared to out-of-plane magnetization, which indicates the presence of easy-plane anisotropy. Films grown on (0 0 1) $SrTiO_3$ substrates show magnetic ordering below T_C ~320 K. On the other hand, films grown on the almost lattice-matched substrates, i.e., films

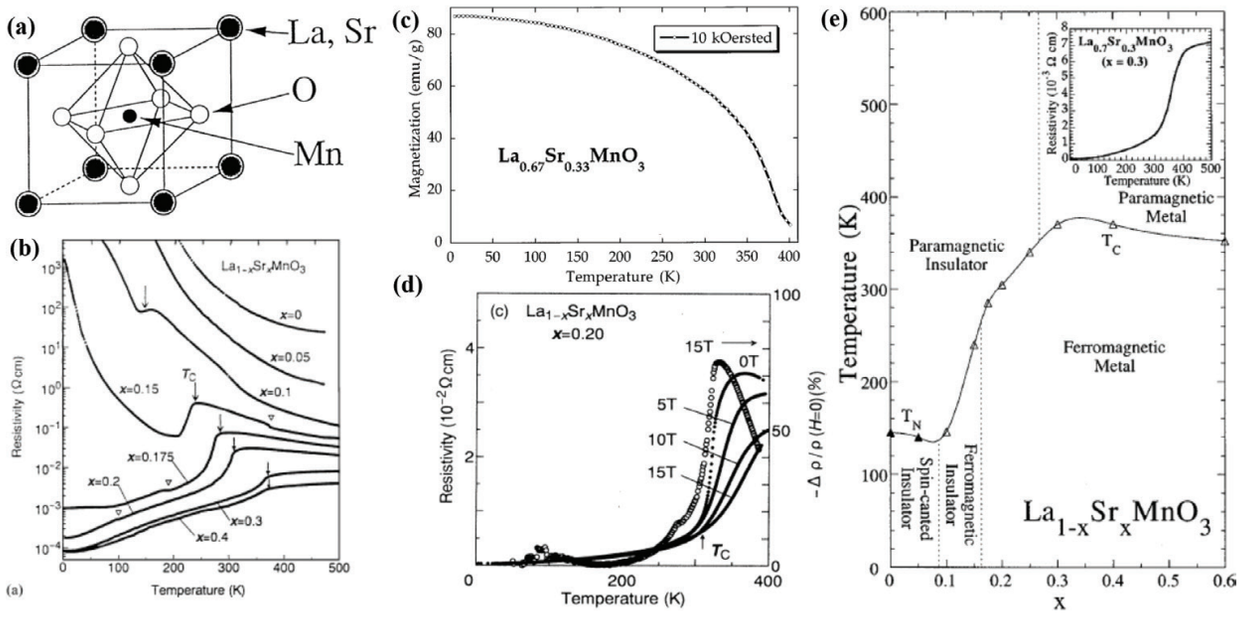

Figure 14. (a) Rhombohedral crystal structure of $La_{0.67}Sr_{0.33}MnO_3$ (LSMO) showing MnO_6 octahedra. (b) Sr hole doping-dependent resistivity of bulk LSMO single crystals showing insulator-to-metal transitions with the kink in resistivity; appearance of magnetic ordering. (c) Magnetization measurements show ferromagnetic ordering above room temperature at T_C ~360 K. (d) Magnetoresistance measurements, i.e., magnetic field-dependent resistivity, show a marked change in resistivity upon the application of a magnetic field, which is defined as the appearance of "colossal magnetoresistance" in LSMO. (e) Temperature- and compositional-dependent phase diagram of LSMO, showing that as Sr hole doping increases, various novel phases can appear in LSMO, making it a rich material that shows complex physics. Adapted and reprinted with permission from Refs. [94, 96, 97, 99]. Copyright 2001 Elsevier Ltd.; Copyright 1995 American Physical Society; Copyright 1996 American Physical Society; Copyright 1996 American Physical Society.

grown on (0 0 1) LSAT and (1 1 0) $NdGaO_3$ substrates, show magnetic ordering below T_C ~340 K. Field-dependent magnetization measurements confirm the presence of perpendicular magnetic anisotropy for films grown on (0 0 1) $LaAlO_3$ substrates, whereas films grown on (0 0 1) $SrTiO_3$ exhibit easy-plane magnetic anisotropy at low T. For the films grown on (0 0 1) LSAT and (1 1 0) $NdGaO_3$ substrates, the presence of distorted easy-pane anisotropy was confirmed by magnetization measurements [103].

Recently, Adamo et al., performed a comprehensive study on the strain effect on the electronic and magnetic properties of LSMO with biaxial strain ranging from −2.3 to +3.2% by using the following substrates: $(1\ 0\ 0)_{pc}$ $LaAlO_3$, (0 0 1) $LaSrGaO_4$, (1 1 0) $NdGaO_3$, (0 0 1) LSAT, (0 0 1) $SrTiO_3$, (1 1 0) $DyScO_3$, (1 1 0) $GdScO_3$, (1 1 0) $SmScO_3$ and (1 1 0) $NdScO_3$ (**Figure 15a–c**) [108]. ρ show a strong strain dependency on the MIT temperature. For low strain values, low temperature ρ is closer to the single-crystal value. The MIT value for films grown on (1 1 0) $NdGaO_3$ is $T_{MIT} > 390$ K, whereas the MIT transition value for films grown on (0 0 1) $SrTiO_3$ is around $T_{MIT} = 370 \pm 10$ K. Films with high compressive strain show fully insulating behavior over the entire T range (**Figure 15d**). For films under higher tensile strain, at $T = 300$ K, ρ is nearly 1 Ω cm. The magnetization behavior of these films are quite similar to that observed by Tsui et al., The observed magnetic behavior and change in T_C exhibit a strong strain dependence (**Figure 15e**), which is in good agreement with the theoretical predictions of Millis et al. [112].

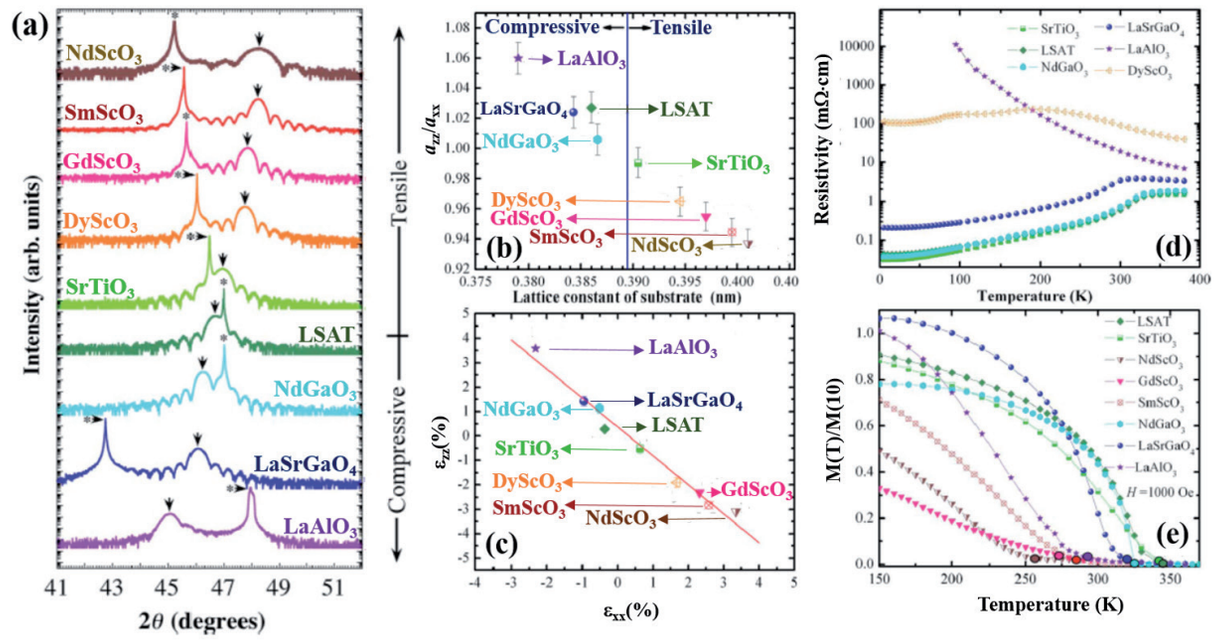

Figure 15. (a) Epitaxial growth of compressive- and tensile-strained $La_{0.67}Sr_{0.33}MnO_3$ (LSMO) films. Films grown on $LaAlO_3$, $LaSrGaO_4$, $NdGaO_3$, and LSAT are subject to compressive strain, whereas films grown on $SrTiO_3$, $DyScO_3$, $GdScO_3$, $SmScO_3$, and $NdScO_3$ are subject to tensile strain. The appearance of thickness fringes in the X-ray diffraction patterns shows the high crystallinity of each film. (b) Change in lattice parameter and (c) evolution of biaxial strain with the judicial choice of substrates for LSMO thin films. (d and e) Resistivity and magnetization of compressive- and tensile-strained films. Highly tensile- or compressive-strained films show insulating behavior (due to the strain and intrinsic atomic disorder effect), whereas metallic behavior was obtained for films that were exposed to moderate tensile or compressive strain. Magnetization measurements show that the ferromagnetic ordering temperature decreases as the tensile strain increases. Reprinted with permission from Ref. [108]. Copyright 2009 AIP Publishing LLC.

4.4. A multiferroic oxide: $BiFeO_3$

Bismuth ferrite, $BiFeO_3$ (BFO), is probably the most promising compound in condensed matter physics [9]. It possess a rhombohedral distorted perovskite structure ($a = b = c = 5.63$ Å, $\alpha = \beta = \gamma = 59.4°$) with space group $R\bar{3}c$ at $T = 300$ K (**Figure 16a**) [113–115]. There is a coexistence of its magnetism and ferroelectricity, that's why $BiFeO_3$ is called a multiferroic (**Figure 16b** and **c**) [115]. In principle, the coexistence of ferroelectricity and magnetism is a very rare phenomenon as ferroelectricity requires B-site ions with d^0 electronic configurations, whereas magnetism requires B-site ions with d^n ($n > 0$) electronic configurations [116]. Therefore, multiferrocity is a very unique phenomenon in condensed matter physics. Bulk single-crystal $BiFeO_3$ shows G-type antiferromagnetic ordering below the Néel temperature at $T_N = 643$ K [117]. In $BiFeO_3$, Fe moments are coupled ferromagnetically with the pseudo-cubic $\{1\ 1\ 1\}_C$ planes, whereas they are antiferromagnetically coupled between neighboring planes. In the bulk, an additional long-range cycloidal magnetic modulation is superimposed on the antiferromagnetic ordering, which results in a rotation of the spin axis through the crystal [43]. It also exhibits ferroelectricity below $T_C \sim 1103$ K with a polarization (P) value of ~3.5 μC/cm² along $(001)_C$ and ~6.1 μC/cm² along $[1\ 1\ 1]_C$ [118]. Recently, the polarization value of highly pure single-crystal $BiFeO_3$ was found to be ~100 μC/cm² along the $[1\ 1\ 1]_C$ [119]. Due to its

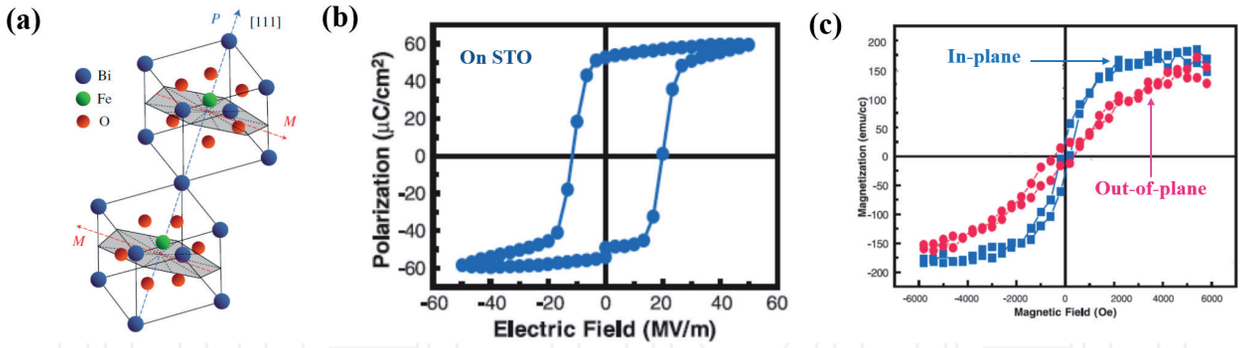

Figure 16. (a) Atomic and magnetic structure of rhombohedral $BiFeO_3$ showing rhombohedral distortion with easy-axis polarization along the $[1\ 1\ 1]_C$ and magnetization plane is perpendicular to the polarization direction. (b) Polarization-electric field hysteresis loop showing that $BiFeO_3$ is ferroelectric with a polarization value of ~60 μC/cm² along the $[1\ 1\ 1]_C$. (c) Magnetization vs. magnetic field hysteresis loop of $BiFeO_3$, showing that the system is antiferromagnetic with a saturation magnetization of ~150 emu/cm³. Blue: in-plane, and red: out-of-plane magnetization-magnetic field loop. Reprinted and adapted with permission [114, 115]. Copyright 2011 The Royal Society; Copyright 2003 American Association for the Advancement of Science.

multiferroic properties above T = 300 K, it is a very promising candidate for room-temperature magnetoelectric device applications [120].

Wang et al., were the first to synthesize high quality epitaxial $BiFeO_3$ heterostructures on (0 0 1) $SrTiO_3$ substrates by using the PLD method and observed multiferroic properties [115]. They observed that these films display a spontaneous P ~ 60 μC/cm² at T = 300 K, an order of magnitude higher than the bulk value. After this finding, it has been shown that the structural, polar, and magnetic behavior of $BiFeO_3$ thin films are highly sensitive to substrate-induced strain, i.e., the strain promoted by using different lattice-mismatched substrates [121–137].

As said, at T = 300 K, $BiFeO_3$ adopts rhombohedral symmetry (*R*-phase). With the availability of various substrates, compressive (−) or tensile (+) strain can be induced on the film, which changes its structural symmetry as octahedral tilt is highly sensitive to strain. Commercially available perovskite substrates such as (1 1 0) $YAlO_3$, (0 0 1) $LaAlO_3$, (0 0 1) LAST, (1 1 0) $DyScO_3$, (1 1 0) $GdScO_3$, (1 1 0) $SmScO_3$, (1 1 0) $NdScO_3$ and (1 1 0) $PrScO_3$ impose a strain on $BiFeO_3$ of −6.5%, −4.5%, −2.6%, −0.5%, −0.1%, +0.2%, +0.9% and +1.2%, respectively, -ve sign being the compressive strain and +ve sign corresponds to tensile strain. For cases of low compressive or tensile strain, $BiFeO_3$ shows monoclinic (*M*) phases (**Figure 17a–f**) [120]. In general, for *R*-phase $BiFeO_3$, the ratio of lattice parameters *c*/*a* is ~1. When grown on high lattice-mismatched (0 0 1) $LaAlO_3$ substrate, the ratio of lattice parameters *c*/*a* shows a large increase to a value of ~1.23 [124, 128]. This high *c*/*a* value can be regarded as being similar to a tetragonal (T_G)-phase or super T_G-phase of $BiFeO_3$. Upon imposing even higher compressive strain by using (1 1 0) $YAlO_3$ substrates, $BiFeO_3$ makes a transition to a fully T_G-phase (**Figure 17g**) [124, 134]. The transition from *R*-phase to T_G-phase was thought to be an isosymmetric monoclinic symmetry phase transition [128]. However, it was actually shown that octahedral tilt disappears, and the sudden jump in the *c*/*a* ratio can be attributed to structural relaxation through an out-of-plane shift. In contrast, imposing moderate tensile strain by using high lattice-mismatched (1 1 0) $NdScO_3$ substrates results in $BiFeO_3$ in a novel orthorhombic (*O*) phase [132].

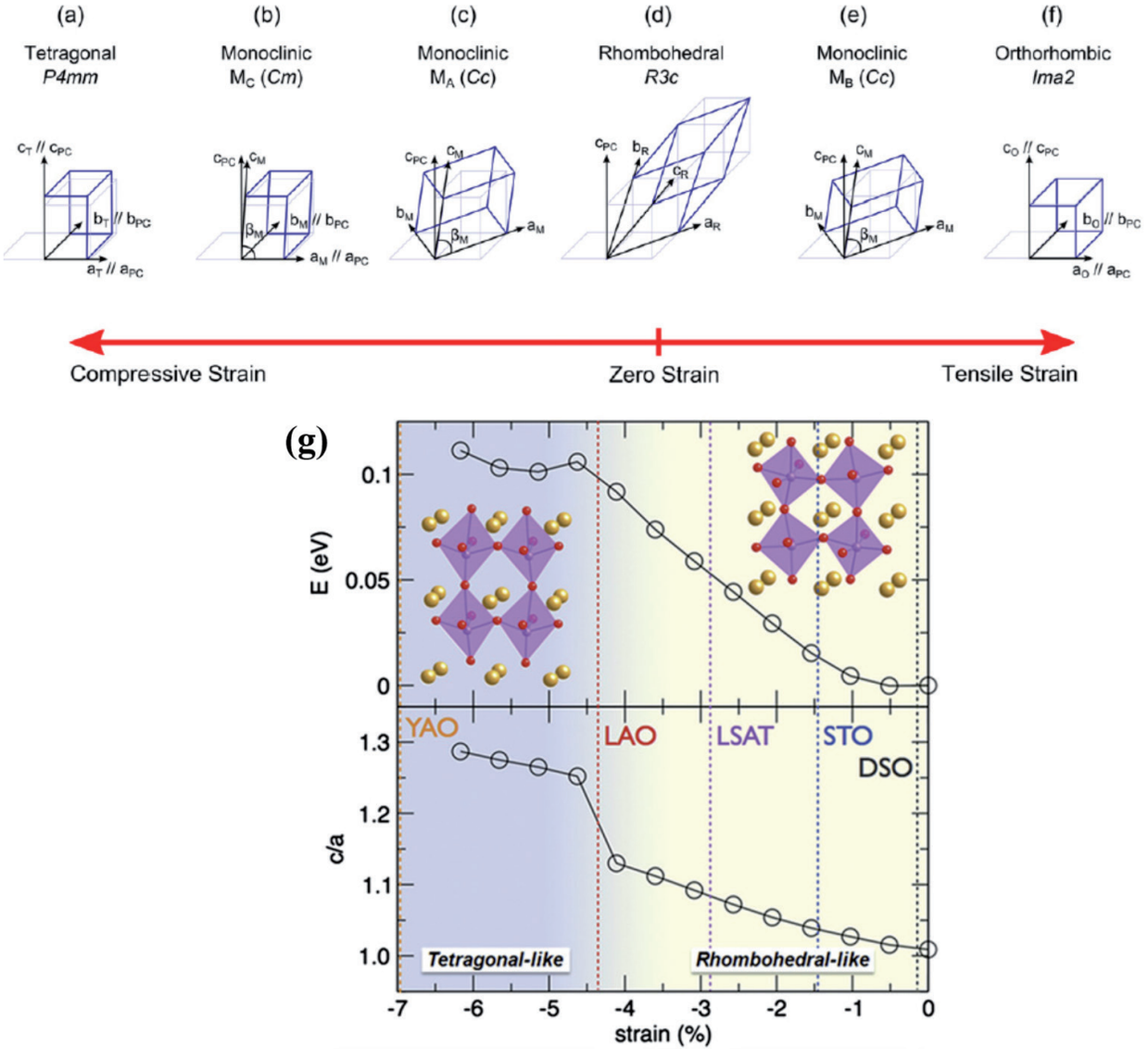

Figure 17. (a–f) Summary of the various crystal structures of $BiFeO_3$ thin films under epitaxial strain, i.e., both compressive and tensile strain. Under different amounts of strain, bulk rhombohedral (*R*) phase to monoclinic (*M*), tetragonal (T_G), and orthorhombic (*O*) phase transitions can be observed in $BiFeO_3$. (g) Calculated overall energy of the system and *c*/*a* ratio for strained $BiFeO_3$. Reprinted with permission from Refs. [120, 124]. Copyright 2014 IOP Publishing Ltd; Copyright 2009 American Association for the Advancement of Science.

First-principle calculations also suggested that with a tensile strain of 2% or more, the orthorhombic phase in $BiFeO_3$ can be stabilized. This is associated with the oxygen octahedral tilt exhibiting short atomic bonds and zig-zag cation displacement patterns. Consequently, the strain effect in $BiFeO_3$ induces very high structural flexibility, which changes the structure from *R*-phase to *M*-, T_G- and *O*-phases or even mixed (*R* + *O*) ones [43, 128, 131].

One of the key aspects of the strain-induced scenario is to increase the out-of-plane *P* in strained $BiFeO_3$ thin films. One of the goals is to induce strain and raise the *P* above 100 μC/cm² at *T* = 300 K. However, in the rhombohedral phase, whatever the growth direction is, the projected *P* along the $[1\ 1\ 1]_C$ increases by only up to ~20% compared to its initial value (**Figure 18a**) [133]. First-principle calculations suggested that suppressing octahedral

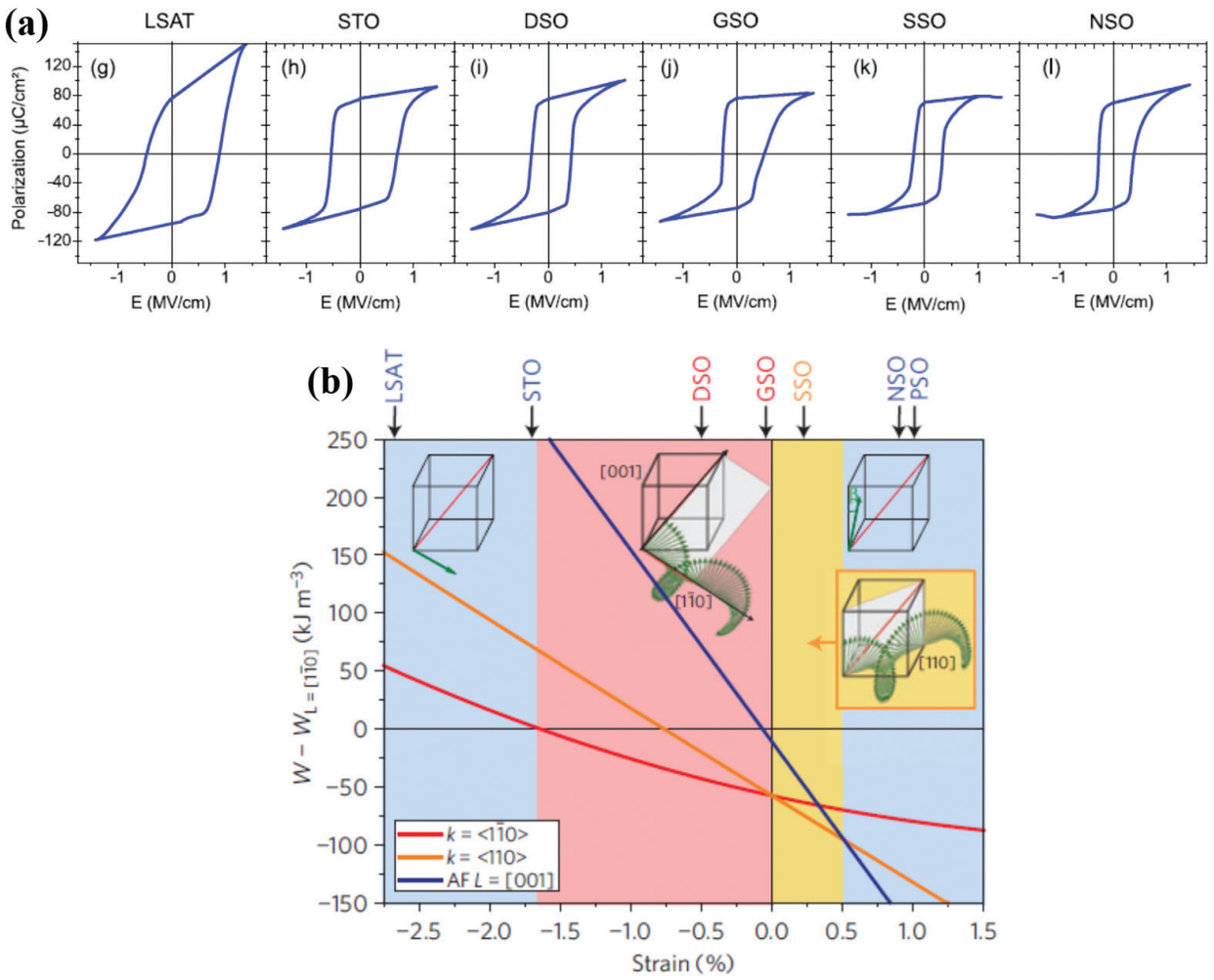

Figure 18. (a) Polarization values of strained $BiFeO_3$ thin films. The large value of polarization for compressively strained films grown on LSAT substrates was attributed to a leakage problem. (b) Magnetic phase diagram shows that with the evolution of strain, various novel magnetic phases can appear in $BiFeO_3$ thin films. The colors correspond to different stable magnetic states (blue: antiferromagnetic; red: type-1 cycloid; orange: type-2 cycloid). The different substrates used for the study are shown above with different colors corresponding to the different magnetic structures of $BiFeO_3$. The spins are denoted by green arrows. Reprinted with permission from Refs. [133, 135]. Copyright 2012 IOP Publishing Ltd; Copyright 2013 Macmillan Publisher Limited.

tilt favors an increase in *P*, whereas the presence of tilts instead favors a change in the direction without changing the *P* [130]. Recent theoretical calculations suggest that if highly strained $BiFeO_3$ is grown with *P4mm* structure, then it would show a high *P* of ~150 μC/cm² along the $[0\ 0\ 1]_C$ and ~100 μC/cm² along the $[1\ 1\ 1]_{C'}$ which has been found experimentally in the super tetragonal-phase [137, 138].

To address how G-type antiferromagnetism is affected by strain effects, Sando et al., studied the strain effect within the range from −2.6% (compressive strain) to +1.0 (tensile strain) for the *R*-phase of $BiFeO_3$ (**Figure 18b**) [135]. By using Mössbauer and Raman spectroscopies combined with Landau–Ginzburg theory and effective Hamiltonian calculations, they observed different magnetic structures for different amounts of strain. For low compressive strain, there exists a bulk-like cycloidal spin modulation with non-collinear order, whereas for moderate tensile strain, they observed a new cycloidal phase with a propagation wave vector

along [110]. For the high compressive- or tensile-strained case, the magnetic state was found to be a pseudo-collinear antiferromagnetic one.

4.5. A conductive oxide interface: $LaAlO_3$-$SrTiO_3$

$SrTiO_3$ and $LaAlO_3$ are both band insulators with band gaps of ~3.25 eV and ~5.6 eV, respectively [139, 140]. Along [0 0 1], $SrTiO_3$ unit cells consist of charge-neutral layers of SrO^0 and TiO_2^0, whereas $LaAlO_3$ consists of polar layers of LaO^{1+} and AlO_2^{1-} (**Figure 19a** and **b**) [14]. In 2004, Ohtomo and Hwang discovered that if band insulator $LaAlO_3$ (LAO) is grown on top of another band insulator, $SrTiO_3$ (STO), with atomic precision, the interface of LAO-STO can be highly conducting, which results in a two-dimensional electron gas (2DEG) at the interface [14]. Surprisingly, conductivity was observed for only one type of interface: LaO-TiO_2 (n-type), whereas insulating characteristics were observed for AlO_2-SrO (p-type) interfaces (**Figure 19c**) [141]. With this discovery, a tremendous interest has emerged among the thin-film community to deposit each and every thin film material with atomically controlled interfaces. Later, it was found that the LAO-STO interface not only is highly conductive but can also show coexistence of superconductivity and magnetism, the quantum Hall effect, and the Rashba effect [18, 142–145]. Based on various experimental observations, the origin of 2DEG, interfacial charge distribution vs. oxygen vacancy scenario is still under debate [146, 147].

Since the atomic configuration of a substrate's topmost layer plays a key role in forming 2DEGs at interfaces between two non-conducting oxides, it would be highly desirable to study the formation of 2DEGs at oxide interfaces with the strain effects [148–155]. Bark et al., grew LAO-STO interfaces on various substrates, such as (1 1 0) $NdGaO_3$, (0 0 1) LSAT, (1 1 0) $DyScO_3$, and (1 1 0) $GdScO_3$ (**Figure 20a**) [148]. By using four different substrates, the strain ranged from compressive to tensile strain as follow; −1.21% compressive strain for films grown on (1 1 0) $NdGaO_3$, −0.96% compressive strain for films grown on (0 0 1) LSAT, +1.11% tensile strain for films grown on (1 1 0) $DyScO_3$, and +1.59% tensile strain for films grown on (1 1 0) $GdScO_3$. They have shown that imposing tensile strain on $SrTiO_3$ destroys the 2DEG, whereas exerting compressive strain leads to the 2DEG nature being retained but with a reduction of carrier concentration compared to that of unstrained LAO-STO interfaces (**Figure 20b**). Using theoretical calculations, they suggested that this behavior is associated with the built-in polarization in $SrTiO_3$, as it was observed that with induced strain, polarization can have built up in pure $SrTiO_3$ as well [44]. This polarization is directed away from the interface and creates a negative polarization opposing that of the polar $LaAlO_3$ layer. It has also been calculated that the distortion of interfacial Ti—O octahedra enhances with increases in in-plane compressive strain, which also modulates the carrier concentration [152]. Applied in-plane compressive strain also reduces the carrier concentration. On the other hand, under tensile strain, the interfacial charge carrier density increases, which is consistent with the theoretical calculations [155]. It has been found that when moving from the compressive-strained to the tensile-strained scenario at the LAO-STO interface, the Ti—O bond length becomes elongated, which confines the Ti d_{xy} orbital electrons at the interface, thus increasing the sheet carrier concentration (n_s) at the interface. For the compressively strained scenario, the Ti—O bond length decreases and the Ti d_{xy} orbital cannot hold all the electrons at the interface; hence, the remaining electrons are transferred to a deeper layer, reducing the carrier concentration at the interface.

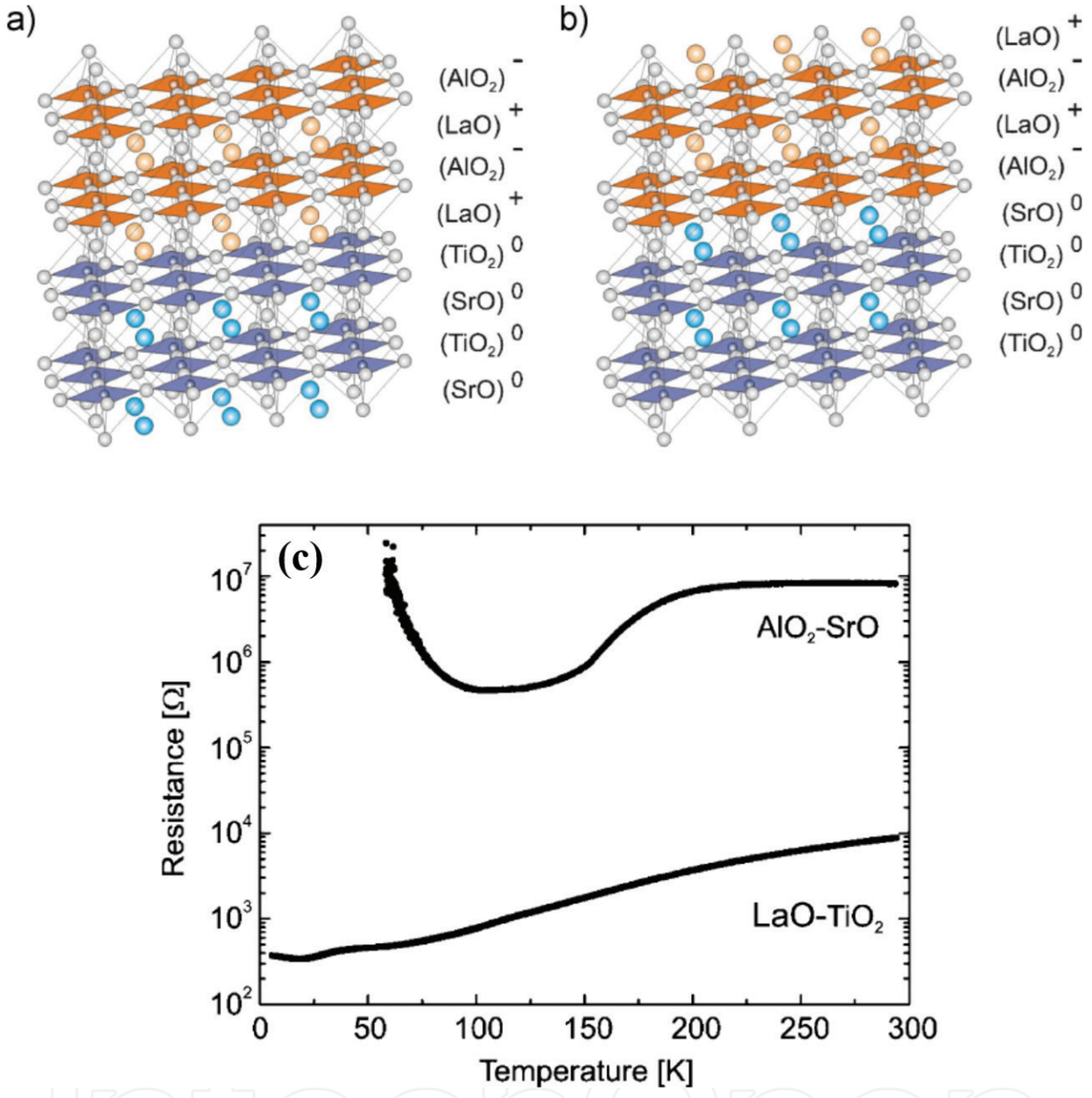

Figure 19. (a) and (b) Schematic representation of two possible interfaces between change neutral $SrTiO_3$ (band insulator) and polar $LaAlO_3$ (band insulator) materials showing the composition and ionic distribution. Depending on the topmost layer termination of the (0 0 1) $SrTiO_3$ substrate, two possible interfaces can form: (1) LaO^{1+}-TiO_2^0, and (2) AlO_2^{1-}-SrO^0. (c) Temperature-dependent resistivity of these two types of interfaces. LaO^{1+}-TiO_2^0 interfaces show metallicity and the formation of 2-dimesnioanl electron gas (2DEG) with n-type charge carriers at the interface, whereas AlO_2^{1-}-SrO^0 interfaces show insulating characteristics at the interface. Reprinted with permission from Refs. [14, 141]. Copyright 2004 Nature Publishing Group; Copyright 2009 WILEY-VCH Verlag GmbH & Co. KGaA, Weinheim.

To observe the correlation and strain effect induced by the topmost polar layer, Ariando et al., grew various combination of polar/non-polar ABO_3 perovskites, e.g., $NaAlO_3/SrTiO_3$, $PrAlO_3/SrTiO_3$, and $NdGaO_3/SrTiO_3$ (**Figure 20c**) [150]. They found that these interfaces are also conducting and form 2DEGs. They also claimed that the interfacial strain and electron correlation caused by the polar layers seem to control the carrier density and mobility at the interface (**Figure 20d**). The presence of large octahedral distortion due to strain also plays an important role in observing

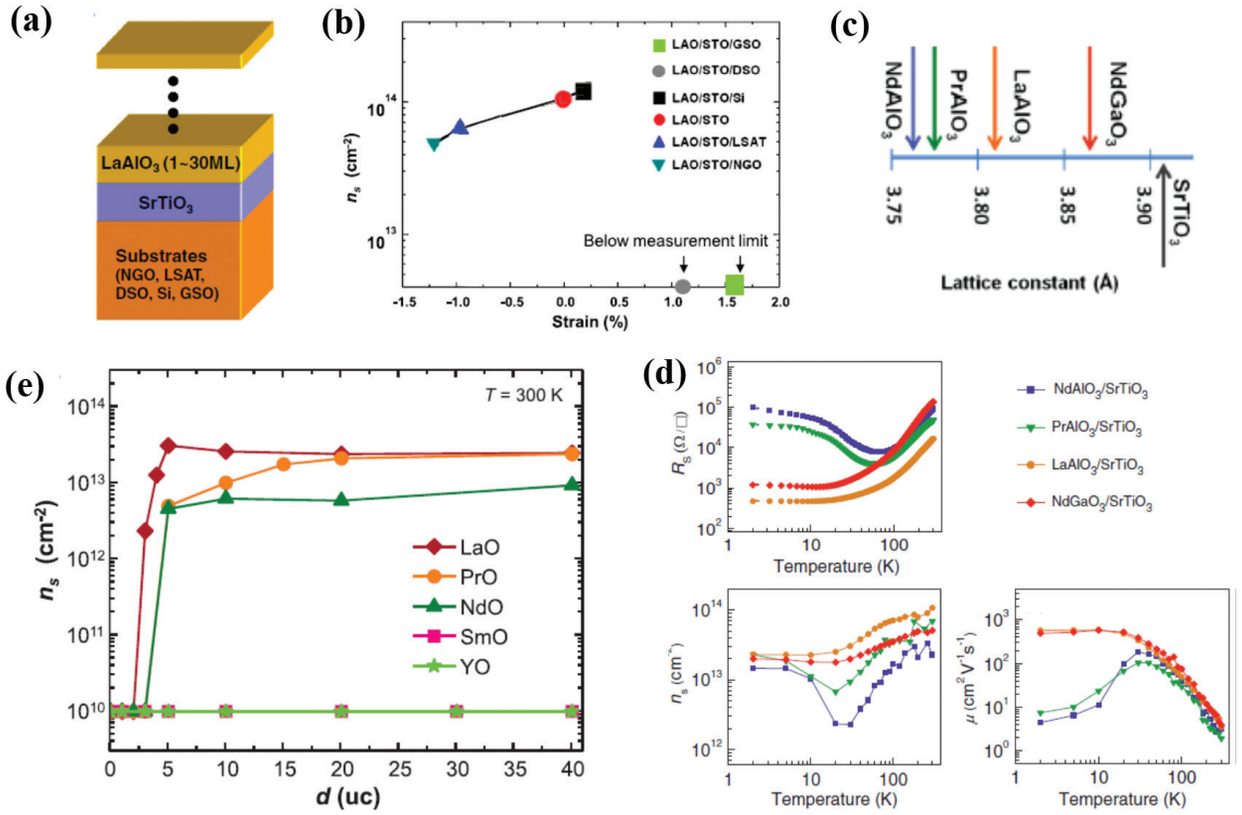

Figure 20. (a) Schematic representation of a $LaAlO_3$-$SrTiO_3$ interface grown on various substrates (i.e., on $GdScO_3$, $DyScO_3$, LSAT and $NdGaO_3$). (b) Carrier concentration at room temperature at the LAO-STO interface under various epitaxial strains. For tensile-strained films, the carrier concentration is below the measurement limit. (c) The strain effect at the interface and lattice parameters of various perovskites. (d) Sheet resistance (R_S), carrier concentration (n_s), and mobility (μ) of various polar/non-polar interfaces. (e) Carrier concentration at the interface of LAO-STO with monolayer growth of rare earth oxides. For some rare earth cases, the interfaces are conductive, whereas insulating interfaces are formed in some cases involving rare-earth oxides, showing the effect of correlation on the formation of 2DEGs at interfaces. Reprinted with the permission from Refs. [148–150]. Copyright 2011 National Academy of Sciences; Copyright 2011 American Association for the Advancement of Science; Copyright 2012 American Physical Society.

these novel phases. Instead of growing various rare earth-based polar ABO_3 perovskites, Jang et al., directly grew monolayers of rare-earth oxides (*R*O, R = La, Pr, Nd, Sm, and Y) to observe the correlation effect at interfaces (**Figure 20e**) [149]. Surprisingly, they found that some oxides (La, Pr, and Nd) forms 2DEGs at the interface, whereas an insulating interface is formed in the case of SmO and YO. Based on the observations and theoretical calculations, they claimed that this is due to the correlation effect at the interface. Independent theoretical calculation also suggest that in-plane strain can induce metal-insulator transitions at oxide interfaces [155].

4.6. A strongly correlated metal: $LaNiO_3$

The physics of strongly correlated materials, i.e., those having strong electronic correlations, is remarkably rich and complex and cannot be understood within the framework of conventional theories of metals and insulators [21, 22]. For example, in strongly correlated nickelate materials, spin, lattice charge, and orbital degrees of freedom result in competing interactions. Due to this, these materials show exotic phases [156–158]. Among strongly correlated materials,

nickelates, more specifically $LaNiO_3$ is a strongly correlated Mott metal [159, 160]. $LaNiO_3$ has a highly distorted rhombohedral structure with lattice parameters of $a = b = 5.4573$ Å, $c = 13.1462$ Å, and $\alpha = \beta = \gamma = 60.49°$ and with space group $R\bar{3}c$ (**Figure 21a**) [161]. Its pseudo-cubic lattice constant is $a_{pc} = 3.84$ Å. It is highly metallic over the entire temperature range (**Figure 21b**) [162]. It is the only member in the perovskite nickelate family ($RENiO_3$, RE = rare earths) which shows no long-range magnetic ordering [156–158].

The functionalities of strongly correlated rare-earth nickelates are highly sensitive to external perturbation, e.g., chemical pressure and atmospheric pressure [156–158]. Thus, it would be very interesting to investigate the ability of strain-based perturbation (i.e., by using various lattice-mismatched substrates) to obtain novel functionalities in $LaNiO_3$. Several groups have reported the strain dependent transport properties in epitaxial $LaNiO_3$ thin films [163–172]. Moon et al., investigated in detail the transport properties of tensile- and compressive-strained $LaNiO_3$ systems. They grew 10-unit cell ultra-thin $LaNiO_3$ films on (1 1 0) $YAlO_3$, (0 0 1) $SrLaAlO_4$, (0 0 1) $LaAlO_3$, (0 0 1) $SrLaGaO_4$, (0 0 1) LSAT, (0 0 1) $SrTiO_3$, and (1 1 0) $GdScO_3$ substrates (**Figure 22a**) [167–169]. They investigated ρ of tensile-strained films and observed that when the tensile strain increases, $LaNiO_3$ gradually evolves from the Mott to the Mott-Anderson regime; i.e., correlation and disorder play a crucial role at low temperature (**Figure 22b**) [163, 167].

The authors have also investigated the Hall effect ($1/R_H \propto T$; R_H = Hall coefficient) in both the compressive- and tensile-strained cases (**Figure 22c**) [168]. They claimed that the evolution of the linear T dependent transport coefficient is quite similar to that of hole-doped cuprate superconductors. By using density functional theoretical (DFT) calculations, they claimed that strain-induced changes in transport properties arise from changes in the low-energy electronic band structure that induces self-doping, i.e., a transfer of charge between the O p and Ni d states. Using detailed quantitative structural analysis and theoretical calculations May et al., found that strain systematically modifies both the Ni—O—Ni bond angles and Ni—O lengths in this functional perovskite oxide (**Figure 22d**) [164, 172], which has strong effect on its strain-dependent transport properties.

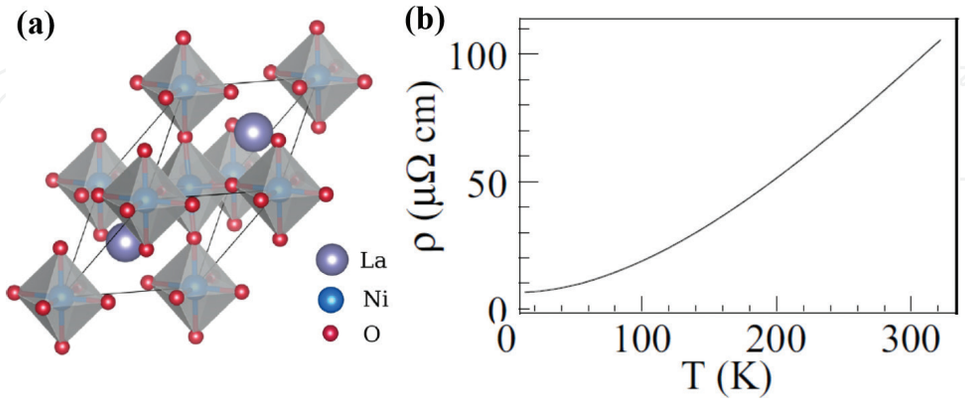

Figure 21. (a) Schematic representation of the distorted rhombohedral crystal structure of $LaNiO_3$ showing highly distorted NiO_6 octahedra with lattice parameters of $a = b = 5.4573$ Å and $c = 13.1462$ Å. The pseudo-cubic unit cell is ~3.84 Å. (b) Resistivity of bulk polycrystalline $LaNiO_3$ showing it is a paramagnetic metal without any indication of magnetic ordering over the entire temperature range. Reprinted with permission from Refs. [161, 162]. Copyright 2015 Elsevier B. V. Ltd.; Copyright 2014 American Physical Society.

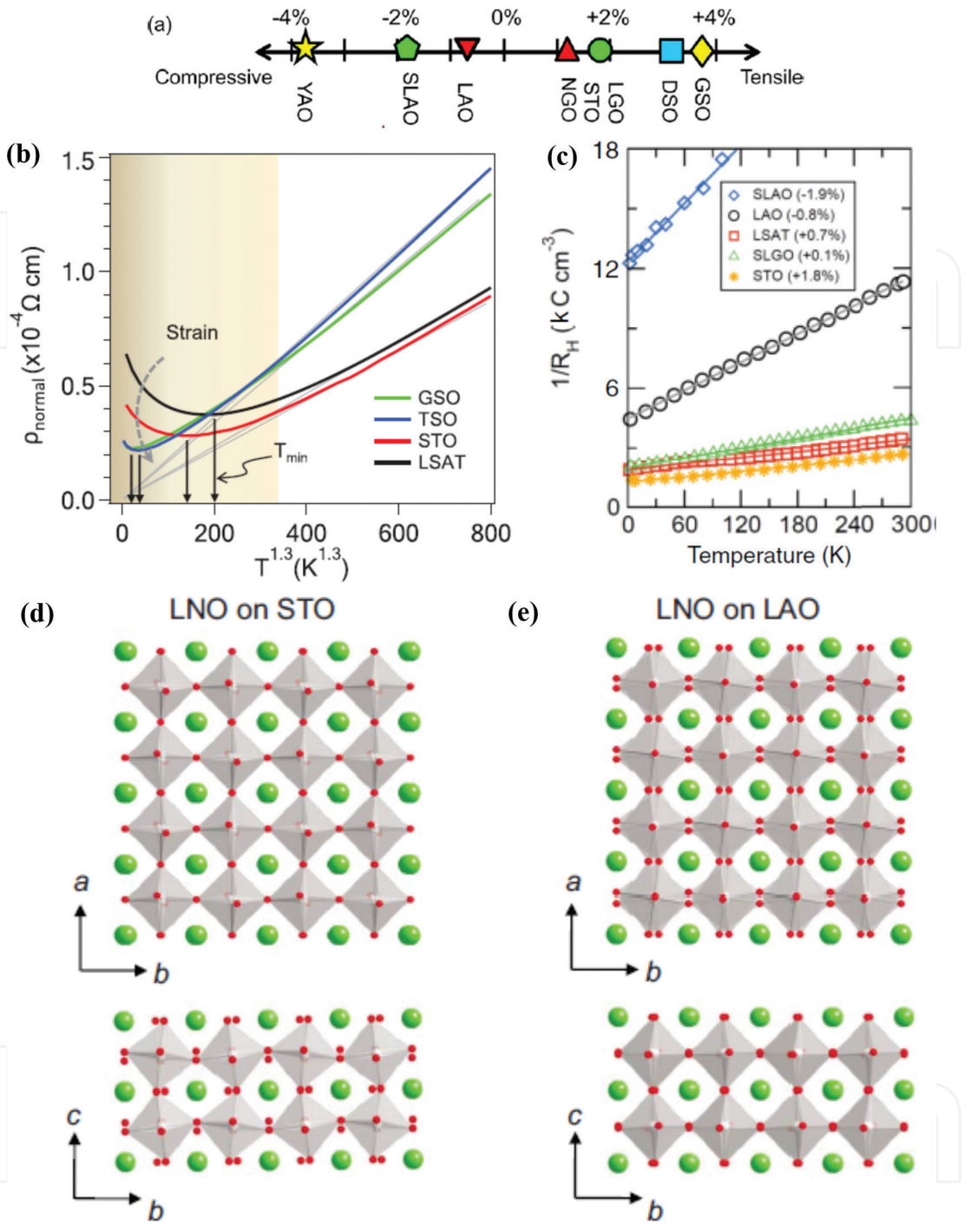

Figure 22. (a) Schematic representation of compressive and tensile strain imposed on $LaNiO_3$ by various metal oxide substrates. (b) Low-temperature resistivity of strained $LaNiO_3$ films. With an increase in tensile strain, resistivity at room temperature increases, although the resistivity minima also decrease. (c) The temperature-dependent Hall coefficient ($1/R_H$) for strained $LaNiO_3$ films grown on various substrates. With an increase in compressive strain, $1/R_H$ becomes almost linearly dependent on temperature ($1/R_H \propto T$), thus bearing a striking resemblance to the behavior of cuprate superconductors. (d) Tensile strain increases rotation of octahedra along the [1 0 0] and [0 1 0], and decreases it along the [0 0 1]. (e) Compressive strain reduces the rotation along the [1 0 0] and [0 1 0], and increases it along the [0 0 1]. Reprinted with permission from Refs [164, 167, 168]. Copyright 2010 American Physical Society; Copyright 2013 American Chemical Society; Copyright 2011 IOP Publishing Ltd and Deutsche Physikalische Gesellschaft.

5. Summary

In principle, material functionalities arise from the coupling between spin, lattice, charge, and orbital degrees of freedom. Lattice strain is thus found to be a unique way to engineering the functionalities of many TMOs, which modifies above energy scales. Here, we presented the effect of strain-dependent functionalities of various TMO-based thin films: (1) a high temperature superconductor, $La_{1.85}Sr_{0.15}CuO_4$, (2) a highly conductive oxide, $SrRuO_3$, (3) a colossal magnetoresistive metal, $La_{0.67}Sr_{0.33}MnO_3$, (4) a multiferroic oxide, $BiFeO_3$, (5) a conducting oxide interface, $LaAlO_3$-$SrTiO_3$, and (6) a strongly correlated metal, $LaNiO_3$. The aforementioned materials all show rich and complex structural, electronic, magnetic and polar phase diagrams that are dependent on epitaxial strain, which is mainly caused by modifications of their crystal structures and the effects of these modification on the coupling of their various degrees of freedoms (relevant energy scales). More specifically, tailoring the shape, size, and position of BO_6 octahedra by strain give rise to new functionalities in ABO_3 perovskite oxides. Strain-dependent MITs, increase in magnetic transition temperature and ferroelectric polarization can be observed in these materials. Obtaining novel properties by designing artificial oxide heterostructures and the subsequent new physics resulting from the strain effect have always been an interesting topic of research among the thin-film community as cheap and environment friendly oxide thin film-based electronic devices are highly in demand in industry. Although there has been vast progress in the strain-dependent tuning of material properties, there is still long way to go to fully understand the intrinsic mechanisms and theoretical developments behind these strain-dependent phenomena. Nevertheless, strain has provided an avenue to explore materials with novel functionalities. We believe that our experimental investigations along with insightful explanations will provide readers with an easier way to understand the strain effect in epitaxial oxide heterostructures and utilize it to explain the fundamental physics and to commercialize oxide-based electronic devices.

Acknowledgements

YHJ was supported by the National Research Foundation (NRF) of Korea (SRC-2011-0030786 and 2015R1D1A1A02062239).

Author details

Abhijit Biswas and Yoon Hee Jeong*

*Address all correspondence to: yhj@postech.ac.kr

Department of Physics, Pohang University of Science Technology, Pohang, Republic of Korea

References

[1] Ashcroft NW, Mermin DN. Solid State Physics. 1st ed. New York: Holt, Rinehart and Winston; 1976. 826 p. DOI: 10.1002/piuz.19780090109

[2] Zachariev ZT, editor. Polycyrstalline Materials—Theoretical and Practical Aspects. 1st ed. Croatia: InTech; 2012. DOI: 10.5772/1391

[3] Rudolph P, editor. Handbook of Crystal Growth: Bulk Crystal Growth. 2nd ed. North-Holland: Elsevier; 2015. 1418 p. ISBN: 978-0-444-63303-3

[4] http://wolfweb.unr.edu/homepage/yjiang/jixi_zhang.html

[5] Kuech T, editor. Handbook of Crystal Growth: Thin Films and Epitaxy. 2nd ed. North-Holland: Elsevier; 2015. ISBN: 978-0-444-63304-0

[6] Imada M, Fujimori A, Tokura Y. Metal-insulator transitions. Reviews of Modern Physics. 1998;**70**:1039-1263. DOI: 10.1103/RevModPhys.70.1039

[7] Prellier W, Lecoeur P, Mercey B. Colossal-magnetoresistive manganite thin films. Journal of Physics: Condensed Matter. 2001;**13**:R915. DOI: 10.1088/0953-8984/13/48/201

[8] Norton DP. Synthesis and properties of epitaxial electronic oxide thin-film materials. Materials Science and Engineering Reports. 2004;**43**:139-247. DOI: 10.1016/j.mser.2003.12.002

[9] Ramesh R, Spaldin NA. Multiferroics: Progress and prospects in thin films. Nature Materials. 2007;**6**:21-29. DOI: 10.1038/nmat1805

[10] Blamire G, MacManus-Driscoll JL, Mathur ND, Barber ZH. The materials science of functional oxide thin films. Advanced Materials. 2009;**21**:3827-3840. DOI: 10.1002/adma.200900947

[11] Martin LW, Schlom DG. Advanced synthesis techniques and routes to new single-phase multiferroics, Current Opinion in Solid State & Materials Science. 2012;**16**:199-215. DOI: 10.1016/j.cossms.2012.03.001

[12] Monkman EJ, Adamo C, Mundy JA, Shai DE, Harter JW, Shen D, Burganov B, Muller DA, Schlom DG, Shen KM. Quantum many-body interaction in digital oxide superlattices. Nature Materials. 2012;**11**:855-859. DOI: 10.1038/nmat3405

[13] Yu P, Chu YH, Ramesh R. Oxide interfaces: Pathway to novel phenomena. Materials Today. 2012;**15**:320-327. DOI: 10.1016/S1369-7021(12)70137-2

[14] Ohtomo A, Hwang HY. A high-mobility electron gas at the $LaAlO_3/SrTiO_3$ heterointerface. Nature (London). 2004;**427**:423-426. DOI: 10.1038/nature02308

[15] Dawber M, Bousquet E. New developments in artificially layered ferroelectric oxide superlattices. MRS Bulletin. 2013:**38**:1048-1055. DOI: 10.1557/mrs.2013.263

[16] Nagaosa N, Sinova J, Onoda A, MacDonald AH, Ong NP. Anomalous Hall effect. Reviews of Modern Physics. 2010;**82**:1539-1592. DOI: 10.1103/RevModPhys.82.1539

[17] Zubko P, Gariglio S, Gabay M, Ghosez P, Triscone JM. Interface physics in complex oxide heterostructures. Annual Review of Condensed Matter Physics. 2011;**2**:141-165. DOI: 10.1146/annurev-conmatphys-062910-140445

[18] Hwang HY, Iwasa Y, Kawasaki M, Keimer B, Nagaosa N, Tokura Y. Emergent phenomena at oxide interfaces. Nature Materials. 2012;**11**:103-113. DOI: 10.1038/nmat3223

[19] Krempa WW, Chen G, Kim YB, Balents L. Correlated quantum phenomena in the strong spin-orbit regime. Condensed Matter Physics. 2014;**5**:57-82. DOI: 10.1146/annurev-conmatphys-020911-125138

[20] Zhang J, Averitt RD. Dynamics and control in complex transition metal oxides. Annual Review of Materials Research. 2014;**44**:19-43. DOI: 10.1146/annurev-matsci-070813-113258

[21] Tokura Y. Correlated-electron physics in transition-metal oxides. Physics Today. 2003;**56**:50-55. DOI: 10.1063/1.1603080

[22] Dagotto E. Complexity in strongly correlated electronic systems. Science. 2005;**309**:257-262. DOI: 10.1126/science.1107559

[23] Tokura Y, Nagaosa N. Orbital physics in transition-metal oxides. Science. 2000;**288**:462-468. DOI: 10.1126/science.288.5465.462

[24] Cheong SW. Transition metal oxides: The exciting world of orbitals. Nature Materials. 2007;**6**:927-928. DOI: 10.1038/nmat2069

[25] Pan L, Zhu G, editors. Perovskite Materials - Synthesis, Characterisation, Properties, and Applications, 1st ed. Croatia: InTech; 2016. DOI: 10.5772/60649. ISBN: 978-953-51-2245-6

[26] Johnsson M, Lemmens P. Perovskites and thin films-crystallography and chemistry. Journal of Physics: Condensed Matter. 2008;**20**:264001. DOI: 10.1088/0953-8984/20/26/264001

[27] Goldschmidt VM. Die Gesetze der Krystallochemie. Naturwissenschaften. 1926;**14**:477-485. DOI: 10.1007/BF01507527

[28] Schlom DG, Chen LQ, Pan X, Schmehl A, Zurbuchen MA. A thin film approach to engineering functionality into oxides. Journal of the American Ceramic Society. 2008;**91**:2429-2454. DOI: 10.1111/j.1551-2916.2008.02556.x

[29] Dijkkamp D, Venkatesan T, Wu XD, Shaheen SA, Jisrawi N, Min-Lee YH, Mclean WL, Croft M. Preparation of Y-Ba-Cu oxide superconductor thin films using pulsed laser evaporation from high T_c bulk material. Applied Physics Letters. 1987;**51**:619-621. DOI: 10.1063/1.98366

[30] Chrisey DB, Hubler GK. Pulsed Laser Deposition of Thin Films. 1st ed. John Wiley & Sons, New York; 1994. 648 p. ISBN: 0-471-59218-8

[31] Christen HM, Eres G. Recent advances in pulsed-laser deposition of complex oxides. Journal of Physics: Condensed Matter. 2008;**20**:264005-264020. DOI: 10.1088/0953-8984/20/26/264005

[32] Koster G, Huijben M, Rijnders G, editors. Epitaxial Growth of Complex Metal Oxides. 1st ed. Elsevier Science & Technology, United Kingdom; 2015. 504 p. ISBN: 978-1-78242-245-7

[33] Opel M. Spintronic oxide grown by laser-MBE. Journal of Physics D: Applied Physics. 2012;**45**:033001-033031. DOI: 10.1088/0022-3727/45/3/033001

[34] McCray WP. MBE deserves a place in the history books. Nature Nanotechnology. 2007;**2**:259-261. DOI: 10.1038/nnano.2007.121

[35] Cho AY, Arthur JR Jr. Molecular beam epitaxy. Progress in Solid State Chemistry. 1975;**10**:157-192. DOI: 10.1016/0079-6786(75)90005-9

[36] Moustakas TD. Molecular beam epitaxy: Thin film growth and surface studies. MRS Bulletin. 1988;**13**:29-36. DOI: 10.1557/S0883769400063892

[37] Nie YF, Zhu Y, Lee CH, Kourkoutis LF, Mundy JA, Junquera J, Ghosez P, Baek DJ, Sung S, Xi XX, Shen KM, Muller DA, Schlom DG. Atomically precise interfaces from non-stoichiometric deposition. Nature Communications. 2014;**5**:4530-4537. DOI: 10.1038/ncomms5530

[38] Phillips JM. Substrate selection for high-temperature superconducting thin films. Journal of Applied Physics. 1996;**79**:1829-1848. DOI: 10.1063/1.362675

[39] Jiang LQ, Guo JK, Liu HB, Zhu M, Zhou X, Wu P, Li CH. Prediction of lattice constant in cubic perovskites. Journal of Physics and Chemistry of Solids. 2006;**67**:1531-1536. DOI: 10.1016/j.jpcs.2006.02.004

[40] Schlom DG, Chen LQ, Eom CB, Rabe KM, Streiffer SK, Triscone JM. Strain tuning of ferroelectric thin films. Annual Review of Materials Research. 2007;**37**:589-626. DOI: 10.1146/annurev.matsci.37.061206.113016

[41] Schlom DG, Chen LQ, Fennie CJ, Gopalan V, Muller DA, Pan X, Ramesh R, Uecker R. Elastic strain engineering of ferroic oxides. MRS Bulletin. 2014;**39**:118-130. DOI: 10.1557/mrs.2014.1

[42] Damodaran AR, Agar JC, Pandya S, Chen Z, Dedon L, Xu R, Apgar B, Saremi S, Martin LW. New modalities of strain-control of ferroelectric thin films. Journal of Physics: Condensed Matter. 2016;**28**:263001-263036. DOI: 10.1088/0953-8984/28/26/263001

[43] Yang Y, Infante IC, Dkhil B, Bellaiche L. Strain effect on multiferroic $BiFeO_3$ films. Comptes Rendus Physique. 2015;**16**:193-203. DOI: 10.1016/j.crhy.2015.01.010

[44] Haeni JH, Irvin P, Chang W, Uecker R, Reiche P, Li YL, Choudhury S, Tian W, Hawley ME, Craigo B, Tagantsev AK, Pan XQ, Streiffer SK, Chen LQ, Kirchoefer SW, Levy J, Schlom DG. Room-temperature ferroelectricity in strained $SrTiO_3$. Nature (London). 2004;**430**:758-761. DOI: 10.1038/nature02773

[45] Lee JH, Fang L, Vlahos LFE, Ke X, Jung YW, Kourkoutis LF, Kim JW, Ryan PJ, Heeg T, Roeckerath M, Goian Bernhagen M, Uecker R, Hammel PC, Rabe KM, Kamba S, Schubert J, Freeland JW, Muller DA, Fennie CJ, Schiffer P, Gopalan V, Halperin EJ, Schlom DG. A strong ferroelectric ferromagnet created by means of spin–lattice coupling. Nature (London). 2010;**466**:954-958. DOI: 10.1038/nature09331

[46] Schlom DG, Mannhart J. Oxide electronics: Interface takes charge over Si. Nature Materials. 2011;**10**:168-169. DOI: 10.1038/nmat2965

[47] Lorentz M, Ramachandra Rao MS, Venkatesan T, Fortunato E, Barquinha P, Branquinho R, Salgueiro D, Martins R, Carlos E, Liu A, Shan FK, Grundmann M, Boschker H, Mukherjee J, Priyadarshini M, DasGupta N, Rogers DJ, Teherani FH, Sandana EV, Bove P, Rietwyk Zaban A, Veziridis A, Weidenkaff A, Muralidhar M, Murakami M, Abel S, Fompeyrine J, Zuniga-Perez J, Ramesh R, Spaldin NA, Ostanin S, Borisov V, Mertig I, Lazenka V, Srinivasan G, Prellier W, Uchida M, Kawasaki M, Pentcheva R, Getenwart P, Miletto Granozio FM, Fontcuberta J, Pryds N. The 2016 oxide electronic materials and oxide interfaces roadmap. Journal of Physics D: Applied Physics. 2016;**49**:433001. DOI: 10.1088/0022-3727/49/43/433001

[48] Rondinelli JM, Spaldin NA. Structure and properties of functional oxide thin films: Insights from electronic-structure calculations. Advanced Materials. 2011;**23**:3363-3381. DOI: 10.1002/adma.201101152

[49] Rondinelli JM, Coh S. Large issosymmetric reorientation of oxygen octahedra rotation axes in epitaxially strained perovskites. Physical Review Letters. 2011;1**06**:235502-235505. DOI: 10.1103/PhysRevLett.106.235502

[50] Rondinelli JM, May SJ, Freeland JW. Control of octahedral connectivity in perovskite oxide heterostructures: An emerging route to multifunctional materials discovery. MRS Bulletin. 2012;**37**:261-270. DOI: 10.1557/mrs.2012.49

[51] Rondinelli JM, Fennie CJ. Octahedral rotation-induced ferroelectricity in cation ordered perovskites. Advanced Materials. 2012;**24**:1961-1968. DOI: 10.1002/adma.201104674

[52] Glazer AM. The classification of tilted octahedra in perovskites. Acta Crystallographica Section A 1972;**B28**:3384-3392. DOI: 10.1107/S0567740872007976

[53] Glazer AM. Simple ways of determining perovskite structures. Acta Crystallographica Section A 1975;**A31**:756-762. DOI: 10.1107/S0567739475001635

[54] Harrison WA. Electronic Structure and the Physical Properties of Solids: The Physics of the Chemical Bonds. 1st ed. New York: Dover; 1989. 608 p. ISBN: 0486660214

[55] Brooks CM, Kourkoutis LF, Heeg T, Schubert J, Muller DA, Schlom DG. Growth of homoepitaxial $SrTiO_3$ thin films by molecular-beam epitaxy. Applied Physics Letters. 2009;**94**:162905-162907. DOI: 10.1063/1.3117365

[56] Bednorz JG, Müller KAZ. Possible high T_c superconductivity in the Ba–La–Cu–O system. Physik B–Condensed Matter. 1986;**64**:189-193. DOI:10.1007/BF01303701

[57] Takagi H, Batlogg B, Kao HL, Kwo J, Cava RJ, Krajewski JJ, Pech WF Jr. Systematic evolution of temperature-dependent resistivity in $La_{2-x}Sr_xCuO_4$. Physical Review Letters. 1992;**69**:2975-2978. DOI: 10.1103/PhysRevLett.69.2975

[58] Cava RJ, Santoro A, Johnson DW, Rhodes WW. Crystal structure of the high-temperature superconductor $La_{0.85}Sr_{0.15}CuO_4$ above and below Tc. Physical Review B. 1987;**35**:6716. DOI: 10.1103/PhysRevB.35.6716

[59] Emery VJ. Theory of high-T_C superconductivity in oxides. Physical Review Letters. 1987;**58**:2794-2797. DOI: 10.1103/PhysRevLett.58.2794

[60] Chang J, Mansson M, Pailhès S, Claesson T, Lipscombe OI, Hayden SM, Patthey L, Tjernberg O, Mesot J. Anisotropc breakdown of Fermi liquid quasiparticle excitations in overdped $La_{2-x}Sr_xCuO_4$. Nature Communications. 2013;**4**:2559-2563. DOI: 10.1038/ncomms3559

[61] Dagotto E. Correlated electrons in high-temperature superconductors. Reviews of Modern Physics. 1994;**66**:763-840. DOI: 10.1103/RevModPhys.66.763

[62] Božović I, He X, Wu J, Bollinger AT. Dependence of the critical temperature in overdoped copper oxides on superfluid density. Nature. 2016;**536**:309-313. DOI: 10.1038/nature19061

[63] Sato H, Naito M. Increase in the superconducting transition temperature by anisotropic strain effect in (0 0 1) $La_{1.85}Sr_{0.15}CuO_4$ thin films on $LaSrAlO_4$ substrates. Physica C. 1997;**274**:221-226. DOI: 10.1016/S0921-4534(96)00675-2

[64] Locquet JP, Perret J, Fompeyrine J, Mächler E, Seo JW, Van Tendeloo G. Doubling the critical temperature of $La_{1.9}Sr_{0.1}CuO_4$ using epitaxial strain. Nature. 1998;**394**:453-456. DOI: 10.1038/28810

[65] Si W, Li HC, Xi XX. Strain and oxygenation effects on superconductivity of $La_{1.85}Sr_{0.15}CuO_4$ thin films. Applied Physics Letters. 1999;**74**:2839-2841. DOI: 10.1063/1.124031

[66] Sato H, Tsukada A, Naito M, Matsuda A. $La_{2-x}Sr_xCuO_y$ epitaxial thin films (x = 0 to 2): Structure, strain, and superconductivity. Physical Review B. 2000;**61**:12447-12456. DOI: 10.1103/PhysRevB.61.12447

[67] Sato H, Tsukada A, Naito M, Matsuda A. La-214 thin films under epitaxial strain. Physica C. 2000;**341**-**248**;1767-1770. DOI: 10.1016/j.physc.2004.03.218

[68] Božović I, Lonvenov G, Belca I, Narimbetov B, Sveklo I. Epitaxial strain and superconductivity in $La_{2-x}Sr_xCuO_4$ thin films. Physical Review Letters. 2002;**89**:107001. DOI: 10.1103/PhysRevLett.89.107001

[69] Sato H. Enhanced superconductivity by reducing magnetism in strained $La_{2-x}Sr_xCuO_4$ films. Physica C. 2008;**468**:2366-2368. DOI: 10.1016/j.physc.2008.09.001

[70] Meyers TL, Jiang L, Park S, Egami T, Lee HN. Strain-relaxation and critical thickness of epitaxial $La_{1.85}Sr_{0.15}CuO_4$ films. APL Materials. 2015;**3**:126102. DOI: 10.1063/1.4937170

[71] Koster G, Klein L, Siemons W, Rijnders G, Steven Dodge J, Eom CB, Blank DHA, Beasley MR. Structure, physical properties, and applications of $SrRuO_3$ thin films. Reviews of Modern Physics. 2012;**84**:253-298. DOI: 10.1103/RevModPhys.84.253

[72] Klein L, Dodge JS, Ahn CH, Reiner JW, Geballe TH, Beasley MR, Kapitulnik A. Transport and magnetization in the badly metallic itinerant ferromagnet $SrRuO_3$. Journal of Physics: Condensed Matter. 1996;**8**:10111-10126. DOI: 10.1088/0953-8984/8/48/026

[73] Allen PB, Berger H, Chauvet O, Forro L, Jarlborg T, Junod A, Revaz B, Santi G. Transport properties, thermodynamics properties, and electronic structure of $SrRuO_3$. Physical Review B. 1996;**53**:4393-4398. DOI: 10.1103/PhysRevB.53.4393

[74] Gan Q, Rao RA, Eom CB, Wu L, Tsui F. Lattice distortion and uniaxial magnetic anisotropy in single domain epitaxial (1 1 0) films of $SrRuO_3$. Journal of Applied Physics. 1999;**85**:5297-5299 DOI: 10.1063/1.369859

[75] Kennedy BJ, Hunter BA. High-temperature phases of $SrRuO_3$. Physical Review B. 1998;**58**:653-658. DOI: 10.1103/PhysRevB.58.653

[76] Cao G, McCall S, Shepard M, Crow JE, Guertin RP. Thermal, magnetic, and transport properties of single-crystal $Sr_{1-x}Ca_xRuO_3$ ($0 \leq x \leq 1.0$). Physical Review B. 1997;**56**:321-329. DOI: 10.1103/PhysRevB.56.321

[77] Mazin II, Singh DJ. Electronic structure and magnetism in Ru-based perovskites. Physical Review B. 1997;**56**:2556. DOI: 10.1103/PhysRevB.56.2556

[78] Kim M, Min BI. Nature of itinerant ferromagnetism in $SrRuO_3$: A DFT + DMFT study. Physical Review B. 2015;**91**:205116. DOI: 10.1103/PhysRevB.91.205116

[79] Funakubo H, Oikawa T, Higashi N, Saito K. Metal organic chemical vapour deposition growth of epitaxial $SrRuO_3$ and $CaRuO_3$ thin films with different orientations as the bottom electrode for epitaxial ferroelectric thin films. Journal of Crystal Growth. 2002;**235**:401-406. DOI: 10.1016/S0022-0248(01)01921-2

[80] Eom CB, Cava RJ, Fleming RM, Phillips JM, van Dover RB, Marshall JH, Hsu JWP, Krajewski JJ, Pecj WF Jr. Single-crystal epitaxial thin films of the isotropic metallic oxides $Sr_{1-x}Ca_xRuO_3$ ($0 \leq x \leq 1$). Science. 1992;**258**:1766-1769. DOI: 10.1126/science.258.5089.1766

[81] Gan Q, Rao RA, Eom CB, Garrett JL, Lee M. Direct measurement of strain effects on magnetic and electrical properties of epitaxial $SrRuO_3$ films. Applied Physics Letters. 1998;**72**:978-980. DOI: 10.1063/1.120603

[82] Chodekar RV, Takamura Y, Suzuki Y. Disorder-induced carrier localization in ultrathin strained $SrRuO_3$ epitaxial films. Journal of Applied Physics. 2006;**99**:08F503. DOI: 10.1063/1.2168437

[83] Zayak AT, Huang X, Neaton JB, Rabe KM. Manipulating magnetic properties of $SrRuO_3$ and $CaRuO_3$ with epitaxial and uniaxial strains. Physical Review B. 2008;**77**:214410. DOI: 10.1103/PhysRevB.77.214410

[84] Vailionis A, Siemons W, Koster G. Room temperature epitaxial stabilization of a tetragonal phase in $ARuO_3$ (A = Ca and Sr) thin films. Applied Physics Letters. 2008;**93**:051909. DOI: 10.1063/1.2967878

[85] Grutter A, Wong F, Arenholz E, Liberati M, Vailinois A, Suzuki Y. Enhanced magnetism in epitaxial $SrRuO_3$ thin films via substrate-induced strain. Journal of Applied Physics. 2010;**107**:09E138. DOI: 10.1063/1.3360345

[86] Choi KJ, Baek SH, Jang HW, Belenky LJ, Lyubchenko M, Eom CB. Phase-transition temperature of strained single-crystal $SrRuO_3$ thin films. Advanced Materials. 2010;**22**:759-762. DOI: 10.1002/adma.200902355

[87] Dirsyte R, Schwarzkopf J, Schmidbauer M, Wagner G, Irmsccher K, Anooz SB, Fornari R. Impact of epitaxial strain on the ferromagnetic transition temperature of $SrRuO_3$ thin films. Thin Solid Films. 2011;**519**:6264-6268. DOI: 10.1016/j.tsf.2011.03.132

[88] Vailionis A, Boschker H, Siemons W, Houwman EP, Blank DHA, Rijnders G, Koster G. Misfit strain accommodation in epitaxial ABO_3 perovskites: Lattice rotations and lattice modulations. Physical Review B. 2011;**83**:064101. DOI: 10.1103/PhysRevB.83.064101

[89] Kan D, Shimakawa Y. Strain effects on structural transition in $SrRuO_3$ epitaxial thin films. Crystal Growth & Design. 2011;**11**:5483-5487. DOI: 10.1021/cg201070n

[90] Kan D, Aso R, Kurata H, Shimakawa Y. Epitaxial strain effect in tetragonal $SrRuO_3$ thin films. Journal of Applied Physics. 2013;**113**:173912. DOI: 10.1063/1.4803869

[91] Herklotz A, Kataja M, Nenkov K, Biegalski MD, Christen HM, Deneke C, Schultz L, Dorr K. Magnetism of the tensile-strain-induced tetragonal state of $SrRuO_3$ films. Physical Review B. 2013;**88**:144412. DOI: 10.1103/PhysRevB.88.144412

[92] Aso R, Kan D, Fujiyoshi Y, Shimakawa Y, Kurata H. Strong dependence of oxygen octahedral distortions in $SrRuO_3$ films on types of substrate-induced epitaxial strain. Crystal Growth & Design. 2014;**14**:6478-6485. DOI: 10.1021/cg501340e

[93] Kan D, Aso R, Kurata H, Shimakawa Y. Phase control of a perovskite transition-metal oxide through oxygen displacement at the heterointerface. Dalton Transactions. 2015;**44**:10594-10607. DOI: 10.1039/c4dt03749a

[94] Dagotto E, Hotta T, Moreo A. Colossal magnetoresistive materials: The key role of phase separation. Physics Reports. 2001;**344**:1-153. DOI: 10.1016/S0370-1573(00)00121-6

[95] Moussa F, Hennion M, Rodriguez-Carvajal J, Moudden H, Pinsard L, Revcolevschi A. Spin waves in the antiferromagnet perovskite $LaMnO_3$: A neutron-scattering study. Physical Review B. 1996;**54**:15149. DOI: 10.1103/PhysRevB.54.15149

[96] Urushibara A, Moritomo Y, Arima T, Asamitu A, Kido G, Tokura Y. Insulator-metal transition and giant magnetoresistance in $La_{1-x}Sr_xMnO_3$. Physical Review B. 1995;**51**:14103-14109. DOI: 10.1103/PhysRevB.51.14103

[97] Snyder GJ, Hiskes R, DiCarolis S, Beasley MR, Geballe TH. Intrinsic electrical and magnetic properties of $La_{0.67}Ca_{0.33}MnO_3$ and $La_{0.67}Sr_{0.33}MnO_3$ MOCVD thin films and bulk material. Physical Review B. 1996;**53**:14434-14444. DOI: 10.1103/PhysRevB.53.14434

[98] Haghiri-Gosnet AM, Renard JP. CMR manganites: Physics, thin films and devices. Journal of Physics D: Applied Physics. 2003;**36**:R127-R150. DOI: 10.1088/0022-3727/36/8/201

[99] Martin MC, Shirane G, Endoh Y, Hirota K, Moritomo Y, Tokura Y. Magnetism and structural distortion in the $La_{0.7}Sr_{0.3}MnO_3$ metallic ferromaganet. Physical Review B. 1996;**53**:14285-14290. DOI: 10.1103/PhysRevB.53.14285

[100] Suzuki Y, Hwang HY, Cheong SW, van Dover RB. The role of strain in magnetic anisotropy of manganite thin films. Applied Physics Letters. 1997;**71**:140-142. DOI: 10.1063/1.119454

[101] Wu Y, Suzuki Y, Rüdigger U, Yu J, Kent AD, Nath TK, Eom CB. Magnetotransport and magnetic domain structure in compressively strained colossal magnetoresistance films. Applied Physics Letters. 1999;**75**:2295-2297. DOI: 10.1063/1.124995

[102] Haghiri-Gosnet AM, Wolfman J, Mercey B, Simon C, Lecoeur P, Korzenski M, Hervieu M, Desfeux R, Baldinozzi G. Microstructure and magnetic properties of strained $La_{0.7}Sr_{0.3}MnO_3$ thin films. Journal of Applied Physics. 2000;**88**:4257-4264. DOI: 10.1063/1.1309040

[103] Tsui F, Somak MC, Nath TK, Eom CB. Strain-dependent magnetic phase diagram of epitaxial $La_{0.67}Sr_{0.33}MnO_3$ thin films. Applied Physics Letters. 2000;**76**:2421-2423. DOI: 10.1063/1.126363

[104] Dho J, Kim YN, Hwang YS, Kim JC, Hur NH. Strain-induced magnetic stripe domains in $La_{0.7}Sr_{0.3}MnO_3$ thin films. Applied Physics Letters. 2003;**82**:1434-1436. DOI: 10.1063/1.1556967

[105] Tebano A, Aruta C, Medaglia PG, Tozzi F, Balestrino G, Sidorenko AA, Allodi G, De Renzi R, Ghiringhelli G, Dallera C, Braicovich L, Brookes NB. Strain-induced phase separation in $La_{0.7}Sr_{0.3}MnO_3$ thin films. Physical Review B. 2006;**74**:245116. DOI: 10.1103/PhysRevB.74.245116

[106] Dey P, Nath TK, Taraphder A. Effects of substrate-induced strain on transport and magnetic properties of epitaxial $La_{0.66}Sr_{0.33}MnO_3$ thin films. Applied Physics Letters. 2007;**91**:012511. DOI: 10.1063/1.2750399

[107] Takamura Y, Chopdekar RV, Arenholz E, Suzuki Y. Control of the magnetic and magnetrotrasport properties of $La_{0.67}Sr_{0.33}MnO_3$ thin films. Applied Physics Letters. 2008;**92**:162504. DOI: 10.1063/1.2908051

[108] Adamo C, Ke X, Wang HQ, Xin HL, Heeg T, Hawley ME, Zander W, Schubert J, Schiffer P, Muller DA, Maritato L, Schlom DG. Effect of biaxial strain on the electrical and magnetic properties of (0 0 1) $La_{0.7}Sr_{0.3}MnO_3$ thin films. Applied Physics Letters. 2009;**95**:112504. DOI: 10.1063/1.3213346

[109] Ovsyannikov GA, Petrzhik AM, Borisenko IV, Klimov AA, Ignatov YA, Demodov VV, Nikitov SA. Magnetotransport characteristics of strained $La_{0.7}Sr_{0.3}MnO_3$ epitaxial manganite films. Journal of Experimental and Theoretical Physics. 2009;**108**:48-55. DOI: 10.1134/S1063776109010075

[110] Španková M, Štrbík V, Dobročka E, Chromik Š, Sojková M, Zheng DN, Li J. Characterization of epitaxial LSMO thin films with high Curie temperature prepared on different substrates. Vacuum. 2016;**126**:24-28. DOI: 10.1016/j.vacuum.2016.01.009

[111] Liu GZ, Yang YY, Qiu J, Chen XX, Jiang YC, Yao JL, Zhao M, Zhao R, Gao J. Substrate-related structural, electrical, magnetic and optical properties of $La_{0.7}Sr_{0.3}MnO_3$ films. Journal of Physics D: Applied Physics. 2016;**49**:075309. DOI: 10.1088/0022-3727/49/7/075304

[112] Millis AJ, Darling T, Migliori A. Quantifying strain dependence in "colossal" magnetoresistance manganites. Journal of Applied Physics. 1998;**83**:1588-1591. DOI: 10.1063/1.367310

[113] Kubel F, Schmid H. Structure of a ferroelectric and ferroelastic monodomain crsytal of the perovskite $BiFeO_3$. Acta Crystallographica Section B 1990;**B46**:698-702. DOI: 10.1107/S0108768190006887

[114] Velev JP, Jaswal SS, Tsymbal EY. Multi-ferroic and magnetoelectric materials and Interfaces. Philosophical Transactions of the Royal Society A. 2011;**369**:3069-3097. DOI: 10.1098/rsta.2010.0344

[115] Wang J, Neaton JB, Zheng H, Nagarajan V, Ogale SB, Liu B, Viehland D, Vaithyanathan V, Schlom DG, Waghmare UV, Spaldin NA, Rabe KM, Wuttig M, Ramesh R. Epitaxial $BiFeO_3$ multiferroic thin film heterostructure. Science. 2003;**299**:1719-1722. DOI: 10.1126/science.1080615

[116] Hill NA. Why are there so few magnetic ferroelectrics?. Journal of Physical Chemistry B. 2000;**104**:6694-6709. DOI: 10.1021/jp000114x

[117] Moreau JM, Michel C, Gerson R, James WJ. Ferroelectric $BiFeO_3$ X-ray and neutron diffraction study. Journal of Physics and Chemistry of Solids. 1971;**32**:1315-1320. DOI: 10.1016/S0022-3697(71)80189-0

[118] Teague JR, Gerson R, James WJ. Dielectric hysteresis in single crystal $BiFeO_3$. Solid State Communications. 1970;**8**:1073-1074. DOI: 10.1016/0038-1098(70)90262-0

[119] Lebeugle D, Colson D, Forget Viret M. Very large spontaneous electric polarization in $BiFeO_3$ single crystals at room temperature and its evolution under cycling fields. Applied Physics Letters. 2007;**91**:022907. DOI: 10.1063/1.2753390

[120] Sando D, Barthélémy A, Bibes M. $BiFeO_3$ epitaxial thin films and devices: Past, present and future. Journal of Physics: Condensed Matter. 2014;**26**:473201-473223. DOI: 10.1088/0953-8984/26/47/473201

[121] Zhang JX, Li YL, Wang Y, Liu ZK, Chen LQ, Chu YH, Zavaliche F, Ramesh R. Effect of substrate-induced strains on the spontaneous polarization of epitaxial $BiFeO_3$ thin films. Journal of Applied Physics. 2007;**101**:114105. DOI: 10.1063/1.2743733

[122] Kim DH, Lee HN, Biegalski MD, Christen HM. Effect of epitaxial strain on ferroelectric polarization in multiferroic $BiFeO_3$ films. Applied Physics Letters. 2008;**92**:012911. DOI: 10.1063/1.2830799

[123] Jang HW, Baek SH, Ortiz D, Folkman CM, Das RR, Chi YH, Shafer P, Zhnag JX, Choudhusry S, Vaithyanathan V, Chen YB, Felker DA, Biegalski MD, Rzchowski MS, Pan XQ, Schlom DG, Chen LQ, Ramesh R, Eom CB. Strain-induced polarization rotation in epitaxial (0 0 1) $BiFeO_3$ thin films. Physical Review Letters. 2008;**101**:107602. DOI: 10.1103/PhysRevLett.101.107602

[124] Zeches RJ, Rossell MD, Zhang JX, Hatt AJ, He Q, Yang CH, Kumar A, Wang CH, Melville A, Adamo A, Sheng G, Chu YH, Ihlefeld JF, Erni R, Ederer C, Gopalan V, Chen LQ, Schlom DG, Spaldn NA, Martim LW, Ramesh R. A strain-driven morphotropic phase boundary in $BiFeO_3$. Sicence. 2009;**326**:977-980. DOI: 10.1126/science.1177046

[125] Infante IC, Lisenkov S, Dupé B, Bibes M, Fusil S, Jacquet E, Geneste G, Petit S, Courtial A, Juraszek J, Bellaiche L, Barthélémy A, Dkhil B. Bridging multiferroic phase transitions by epitaxial strain in $BiFeO_3$. Physical Review Letters. 2010;**105**:057601. DOI: 10.1103/PhysRevLett.105.057601

[126] Dupe B, Infante IC, Geneste G, Janolin PE, Bibes M, Berthelemy A, Lisenkov S, Bellaiche L, Ravy S, Dkhil B. Competing phases in $BiFeO_3$ thin films under compressive epitaxial strain. Physical Review B. 2010;**81**:144128. DOI: 10.1103/PhysRevB.81.144128

[127] Huang CW, Chu YH, Chen ZH, Wang J, Sritharan T, He Q, Ramesh R, Chen L. Strain-driven phase transitions and associated dielectric/piezoelectric anomalies in $BiFeO_3$ thin films. Applied Physics Letters. 2010;**97**:152901. DOI: 10.1063/1.3499658

[128] Hatt AJ, Spaldin NA, Ederer C. Strain-induced isosymmetric phase transition in $BiFeO_3$. Physical Review B. 2010;**81**:054109. DOI: 10.1103/PhysRevB.81.054109

[129] Woo CS, Lee JH, Chu K, Jang BK, Kim YB, Koo TY, Yang P, Qi Y, Chen Z, Chen L, Choi HC, Shim JH, Yang CH. Suppression of mixed-phase areas in highly elongated $BiFeO_3$ thin films on $NdAlO_3$ substrates. Physical Review B. 2012;**86**:054417. DOI: 10.1103/PhysRevB.86.054417

[130] Dupé B, Prosandeev S, Geneste G, Dkhil B, Bellaiche L. $BiFeO_3$ films under tensile epitaxial strain from first principles. Physical Review Letters. 2011;**106**:237601. DOI: 10.1103/PhysRevLett.106.237601

[131] Christen HM, Nam JH, Kim HS, Hatt AJ, Spaldin NA. Stress-induced R-M_A-M_C-T symmetry changes in $BiFeO_3$ films. Physical Review B. 2011;**83**:144107. DOI: 10.1103/PhysRevB.83.144107

[132] Yang JC, He Q, Suresha SJ, Kuo CY, Peng CY, Haislmaier RC, Motyka MA, Sheng G, Adamo C, Lin HJ, Hu Z, Chnag L, Tjeng LH, Arenholz E, Podraza NJ, Bernhagen M, Uecker R, Schlom DG, Gopalan V, Chen LQ, Chen CT, Ramesh R, Chu YH. Orthorhombic $BiFeO_3$. Physical Review Letters. 2012;**109**:247606. DOI: 10.1103/PhysRevLett.109.247606

[133] Daumont C, Ren W, Infante IC, Lisenkov S, Allibe J, Carŕeťero C, Fusil S, Jacquet E, Bouvet T, Bouamrane F, Prosandeev S, Geneste G, Dkhil B, Bellaiche L, Barthélémy A, Bibes M. Strain dependence of polarization and piezoelectric response in epitaxial $BiFeO_3$ thin films. Journal of Physics: Condensed Matter. 2012;**24**:162202. DOI: 10.1088/0953-8984/24/16/162202

[134] Liu HJ, Chen HJ, Liang WI, Lee HY, Lin SJ, Chu YH, Structural study in highly compressed $BiFeO_3$ epitaxial thin films on $YAlO_3$. Journal of Applied Physics. 2012;**112**:052002. DOI: 10.1063/1.4746036

[135] Sando D, Agbelele A, Rahmedov D, Liu J, Rovillain P, Toulouse C, Infante IC, Pyatakov AP, Fusil S, Jacquet E, Carrétéro C, Deranlot C, Lisenkov S, Wang D, LeBreton JM, Cazayous M, Sacuto A, Juraszek J, Zvezdin AK, Bellaiche L, Dkhil B, Barthélémy A, Bibes M. Crafting the magnonic and spintronic response of $BiFeO_3$ films by epitaxial strain. Nature Materials. 2013;**12**:641-646. DOI: 10.1038/nmat3629

[136] Sando D, Xu B, Bellaiche L, Nagarajan V. A multiferroic on the brink: Uncovering the nuances of strain-induced transitions in $BiFeO_3$. Applied Physics Reviews. 2016;**3**:011106. DOI: 10.1063/1.4944558

[137] Ederer C, Spadin NA. Effect of epitaxial strain on the spontaneous polarization of thin film ferroelectrics. Physical Review Letters. 2005;**95**:257601. DOI: 10.1103/PhysRevLett.95.257601

[138] Zhen Fan Z, Juanxiu Xiao J, Huajun Liu H, Ping Yang P, Qingqing Ke Q, Wei Ji W, Kui Yao K, Khuong P, Ong KP, Kaiyang Zeng K, John Wang J. Stable ferroelectric perovskite structure with giant axial ratio and polarization in epitaxial $BiFe_{0.6}Ga_{0.4}O_3$ thin films.. ACS Applied Materials and Interfaces. 2015;**7**:2648-2653. DOI: 10.1021/am509016w

[139] van Benthem K, Elsässer C, French RH. Bulk electronic structure of $SrTiO_3$: Experiment and theory. Journal of Applied Physics. 2001;**90**:6156-6164. DOI: 10.1063/1.1415766

[140] Lim SG, Kriventsov S, Jackson TN, Haeni JH, Schlom DG, Balbashov AM, Uecker R, Riche P, Freeouf JL, Lucovsky G. Dielectric functions and optical bandgaps of high-K dielectrics for metal-oxide semiconductor field-effect transistors by far ultraviolet spectroscopic ellipsometry. Journal of Applied Physics. 2002;**91**:4500-4505. DOI: 10.1063/1.1456246

[141] Huijben M, Brinkman A, Koster G, Rijnders G, Hilgenkamp H, Blank DHA. Structure-property relation of $SrTiO_3/LaAlO_3$ interfaces. Advanced Materials. 2009;**21**:1665-1677. DOI: 10.1002/adma.200801448

[142] Li L, Richter C, Mannhart J, Ashoori RC. Coexistence of magnetic order and two-dimensional superconductivity at $LaAlO_3/SrTiO_3$ interfaces. Nature Physics. 2011;**7**:762-766. DOI: 10.1038/nphys2080

[143] Bert JA, Kalisky, Bell C, Kim M, Hikita Y, Hwang HY, Moler KA. Direct imaging of the coexistence of ferromagnetism and superconductivity at the $LaAlO_3/SrTiO_3$ interfaces. Nature Physics. 2011;**7**:767-771. DOI: 10.1038/nphys2079

[144] Trier F, Prawiroatmodjo GEDK, Zhong Z, Christensen DV, von Soosten M, Bhowmik A, Lastra JMG, Chen Y, Jespersen TS, Pryds N. Quantization of hall resistance at the metallic interface between an oxide insulator and $SrTiO_3$. Physical Review Letters. 2016;**117**:096804. DOI: 10.1103/PhysRevLett.117.096804

[145] Caviglia AD, Gabay M, Gariglio S, Reyren N, Cancellieri C, Triscone JM. Tunable rashba spin-orbit interaction at oxide interfaces. Physical Review Letters. 2012;**104**:126803. DOI: 10.1103/PhysRevLett.104.126803

[146] Nakagawa N, Hwang HY, Muller DA. Why some interfaces cannot be sharp. Nature Materials. 2006;**5**:204-209. DOI: 10.1038/nmat1569

[147] Liu ZQ, Li CJ, Lu WM, Huang XH, Huang Z, Zeng SW, Qiu XP, Huang LS, Annadi A, Chen JS, Coey JMD, Ariando VT. Origin of the two-dimensional electron gas at $LaAlO_3/SrTiO_3$ interfaces: The role of oxygen vacancies and electronic reconstruction. Physical Review X. 2013;**3**:021010. DOI: 10.1103/PhysRevX.3.021010

[148] Bark CW, Felker DA, Wnag Y, Zhnag Y, Jang HW, Folkman CM, Park JW, Baek SH, Zhou H, Fong DD, Pan XQ, Tsymbal EY, Rzchowski MS, Eom CB. Tailoring a two-dimensional electron gas at the $LaAlO_3/SrTiO_3$ (001) interfaces by epitaxial strain. PNAS. 2011;**108**:4720-4724. DOI: 10.1073/pnas.1014849108

[149] Jang HW, Felker DA, Bark CW, Wang Y, Niranjan MK, Nelson CT, Zhnag Y, Su D, Folkman CM, Baek SH, Lee S, Janicka K, Zhu Y, Pan XQ, Fong DD, Tsymnal EY, Rzchowski MS, Eom CB. Metallic and insulating oxide interfaces controlled by electronic correlations. Science. 2011;**331**:886-889. DOI: 10.1126/science.1198781

[150] Anandi A, Putra A, Liu ZQ, Wang X, Gopinadhn K, Huang Z, Dhar S, Ariando VT. Electronic correlation and strain effects at the interfaces between polar and nonpolar complex oxides. Physical Review B. 2012;**86**:085450. DOI: 10.1103/PhysRevB.86.085450

[151] Huang Z, Liu ZQ, Yang M, Zeng SW, Anandi A, Lu WM, Tan XL, Chn PF, Sun L, Wang XR, Zhao YL, Li CJ, Zhou J, Han K, Wu WB, Feng YP, Coey JMD. Biaxial strain-induced transport property changes in atomically tailored $SrTiO_3$-based systems. Physical Review B. 2014;**90**:125156. DOI: 10.1103/PhysRevB.90.125156

[152] Nazir S, Behtash M, Yang K. Enhancing interfacial conductivity and spatial charge confinement of $LaAlO_3/SrTiO_3$ heterostructures via strain engineering. Applied Physics Letters. 2014;**105**:1416020. DOI: 10.1063/1.4897626

[153] Fister TT, Zhou H, Luo Z, Seo SSA, Hruszkewycz SO, Proffit DL, Esatman JA, Fuoss PH, Baldo PM, Lee HN, Fong DD. Octahedral rotations in strained $LaAlO_3/SrTiO_3$ (001) heterostructures. APL Materials. 2014;**2**:021102. DOI: 10.1063/1.4865160

[154] Du Y, Wang C, Li J, Zhang X, Wang F, Zhu Y, Yin N, Mei L. The effect of in-plane strain on the electronic properties of $LaAlO_3/SrTiO_3$ interfaces. Computational Materials Science. 2015;**99**:57-61. DOI: 10.1016/j.commatsci.2014.11.039

[155] Nazir S, Behtash M, Yang K. The role of uniaxial strain in tailoring the interfacial properties of $LaAlO_3/SrTiO_3$ heterostructures. RSC Advances. 2015;**5**:15682-15689. DOI: 10.1039/c4ra15866k

[156] Medarde ML, Structural, magnetic and electronic properties of $RNiO_3$ perovskites (R = rare earth). Journal of Physics: Condensed Matter. 1997;**9**:1679-1707. DOI: 10.1088/0953-8984/9/8/003

[157] Catalan G. Progress in perovskite nickelate research. Phase Transitions: A Multinational Journal. 2008;**81**:729-749. DOI: 10.1080/01411590801992463

[158] Middey S, Chakhalian J, Mahadevan P, Freeland JW, Millis AJ, Sarma DD. Physics of ultrathin films and heterostructures of rare-earth nickelates. Annual Review of Materials Research. 2016;**46**:11.1-11.30. DOI: 10.1146/annurev-matsci-070115-032057

[159] Rajeev KP, Shivashankr GV, Raychaudhuri AK. Low-temperature electronic properties of a normal conducting perovskite oxide ($LaNiO_3$). Solid State Communications. 1991;**79**:591-595. DOI: 10.1016/0038-1098(91)90915-I

[160] Sreedhar K, Honig JM, Darwin M, McElfresh M, Shand PM, Xu J, Crooker BC, Spalek J. Electronic properties of the metallic perovskite $LaNiO_3$: Correlated behavior of 3*d* electrons. Physical Review B. 1992;**46**:6382-6386. DOI: 10.1103/PhysRevB.46.6382

[161] Masys Š, Jonauskas V. Elastic properties of rhombohedral, cubic, and monoclinic phases of $LaNiO_3$ by first principle calculations. Computational Materials Science. 2015;**108**:153-159. DOI: 10.1016/j.commatsci.2015.06.034

[162] Zhou JS, Marshall LG, Goodenough JB. Mass enhancement versus Stoner enhancement in strongly correlated metallic perovskites: $LaNiO_3$ and $LaCuO_3$. Physical Review B. 2014;**89**:245138. DOI: 10.1103/PhysRevB.89.245138

[163] Son J, Moetakef P, LeBeau JM, Ouellette D, Balents L, Allen SJ, Stemmer S. Low-dimensional Mott materials: Transport in ultrathin epitaxial $LaNiO_3$ films. Applied Physics Letters. 2010;**96**:062114. DOI: 10.1063/1.3309713

[164] May SJ, Kim JW, Rondinelli JM, Karapetrova E, Spaldin NA, Bhattacharya A, Ryan PJ. Quantifying octahedral rotations in strained perovskite oxide films. Physical Review B. 2010;**82**:014110. DOI: 10.1103/PhysRevB.82.014110

[165] Chakhalian J, Rondinelli JM, Liu J, Gray BA, Kareev M, Moon EJ, Prasai N, Cohn JL, Varela M, Tung IC, Bedzyk MJ, Altendorf SG, Strigari F, Dabrowski B, Tjeng LH, Ryan PJ, Freeland JW. Asymmetric orbital-lattice interactions in ultrathin correlated oxide films. Physical Review Letters. 2011;**107**:11680. DOI: 10.1103/PhysRevLett.107.116805

[166] Stewart MK, Yee CH, Liu J, Kareev M, Smith RK, Chapler BC, Varela M, Ryan PJ, Haule K, Chakhalian J, Basov DN. Optical study of strained ultrathin films of strongly correlated $LaNiO_3$. Physical Review B. 2011;**83**:075125. DOI: 10.1103/PhysRevB.83.075125

[167] Moon EJ, Gray BA, Kareev M, Liu J, Altendorf SG, Strigari F, Tjeng LH, Freeland JW, Chakhalain J. Strain-dependent transport properties of the ultra-thin correlated metal, $LaNiO_3$. New Journal of Physics. 2011;**13**:073037. DOI: 10.1088/1367-2630/13/7/073037

[168] Moon EJ. Rondinelli JM, Prasai N, Gray BA, Kareev M, Chakhalain J, Cohn JL. Strain-controlled band engineering and self-doping in ultrathin $LaNiO_3$ films. Physical Review B. 2012;**85**:121106(R). DOI: 10.1103/PhysRevB.85.121106

[169] Moon EJ, Gray BA, Pimpinelli A, Kareev M, Meyers D, Chakhalain J. Strain-controlled epitaxial stabilization in ultrathin $LaNiO_3$ films grown by pulsed laser deposition. Crystal Growth & Design. 2013;**13**:2256-2259. DOI: 10.1021/cg300958z

[170] Zhu M, Komissinsky P, Radetinac A, Wang Z, Alff L. Joint effect of composition and strain on the anomalous transport properties of $LaNiO_3$ films. Journal of Applied Physics. 2015;**117**:155306. DOI: 10.1063/1.4918661

[171] Weber MC, Gunnou, Dix N, Pesquera D, Sanchez F, Herranz G, Fontcuberta J, López-Conesa L, Estradé S, Peiró F, Iñiguez J, Kreisel J. Multiple strain-induced phase transitions in $LaNiO_3$ thin films. Physical Review B. 2016;**94**:014118. DOI: 10.1103/PhysRevB.94.014118

[172] Misra D, Kundu TK. Strain-controlled transport mechanism in strongly correlated $LaNiO_3$. Journal of Electronic Materials. 2017;**46**:150-157. DOI: 10.1007/s11664-016-4889-3